Development of wind resource assessment methods and application to the Waterloo region

by

Vivian Lam

A thesis
presented to the University of Waterloo
in fulfillment of the
thesis requirement for the degree of
Master of Applied Science
in
Mechanical Engineering

Waterloo, Ontario, Canada, 2013

I hereby declare that I am the sole author of this thesis. This is a true copy of the thesis, including any required final revisions, as accepted by my examiners.

I understand that my thesis may be made electronically available to the public.

Abstract

A wind resource assessment of two sites in the Waterloo region, WRESTRC and RIM Park, was conducted using wind speed, wind direction, temperature and pressure data collected from meteorological towers for over two years. The study was undertaken as part of the W3 Wind Energy Project, and the equipment was purchased from NRG Systems and R. M. Young Company. The data was filtered to reduce the effect of icing and tower shadow, and was analyzed using MATLAB software.

Based on the mean wind speeds, small wind turbines less than 50 kW in capacity would be appropriate at both sites. Wind speeds tended to be stronger during the winter than the summer, and during the afternoon than the rest of the day. Both sites also exhibited a strong dominant wind direction – from the northwest. Due to the terrain, the wind shear and turbulence intensity at WRESTRC were moderate when the wind flowed from the dominant direction, but very high from other directions. The wind shear and turbulence intensity at RIM Park were consistently moderate in all directions. Although the terrain seems more complex at WRESTRC, the wind speed distribution and estimated annual energy production were higher at WRESTRC than at RIM Park, which indicates that it is a more viable site. The estimated capacity factors ranged from 9.4% to 22% depending on the hub height, which is not nearly high enough to suggest a commercial wind farm would be viable at either site. A small 5 kW to 15 kW wind turbine in the Waterloo region could offset the electricity usage of an average home.

A two-parameter power law model of wind shear was explored and compared with the standard one-parameter model. In terms of goodness-of-fit, the two-parameter model did perform better. But in terms of accuracy of extrapolation, it was not conclusively better or worse than a one-parameter model forced through the known data point closest to the prediction height.

The relationship between turbulence intensity and measurement interval was examined. Since atmospheric flow is unsteady, they are not independent. The perceived turbulence intensity was found to increase exponentially with time intervals under 24 hours.

Two linear regression-based Measure-Correlate-Predict methods were evaluated using long-term data from a weather station also at WRESTRC. The ordinary least squares method was considered the baseline given its simplicity. The variance ratio method improved upon it by ensuring that the variance of the wind speed distribution at the target site was preserved.

Acknowledgements

I would like to thank a number of people who have been part of my life over the past four years. Their generous support and contributions have been invaluable.

First, I would like to thank my supervisor, Dr. David Johnson, for allowing me to explore my own area of interest, and for being incredibly kind and patient as I did so. To my fellow graduate students in the Wind Energy Group – Michael McWilliam, Brian Gaunt, Adam McPhee, Kobra Gharali, Erik Skensved, Stephen Orlando, Drew Gertz, Adam Bale, and Nigel Swytink-Binnema – I learned a lot from you and enjoyed the time I spent with you.

I would also like to thank Karen Moyer, Jeff Barten, Brian Bechtel, and everyone who participated in the W3 Wind Energy Project. This thesis would not have been possible without their work.

Finally, I would like to thank my family for their continued emotional and financial support. Every day I am grateful to have been born to such wonderful parents. And to my sister and brother-in-law, thanks for the free meals.

Dedication

This thesis is dedicated to my grandparents, who I did not get to know well, but whose hard work and sacrifice enabled me to enjoy the life and opportunities I've been blessed with.

Table of Contents

List of Tables

List of Figures

Nomenclature

α	Roughness exponent	
α_{1p}	Roughness exponent of the 1-parameter model	
α_{2p}	Roughness exponent of the 2-parameter model	
β	Secondary parameter of the 2-parameter model	
δ	Uncertainty	
λ	Weibull scale parameter	
ρ	Density	kg/m^3
σ_u	Standard deviation wind speed	m/s
$\bar{U}$	Mean wind speed	m/s
$\bar{y}$	Mean value	
$\hat{y}$	Predicted value	
A	Area	m^2
a	IEC wind turbine design parameter	
b	Intercept	
E	Energy	J
f	Frequency	
i	Index in a data set	
I_u	Turbulence intensity	

I_{15}	Turbulence intensity at 15 m/s	
k	Weibull shape parameter	
m	Slope	
N	Number of points in a data set	
P	Power	J/s
p	Pressure	Pa
R	Gas constant	J/kg/°C
T	Temperature	°C
t	Time	s
U	Wind speed	m/s
V	Velocity	m/s
x	Independent variable	
y	Dependent variable	
z	Height above ground	m
z_0	Roughness length	m
z_{ref}	Reference height	m

Chapter 1

Introduction

A wind turbine is a machine that converts the kinetic energy of the wind in to useful forms of energy. Windmills that generate mechanical energy have existed for over 3000 years, while the earliest example of a wind turbine that generates electricity can be found in the late 19th century [1]. In the 1980s, the oil crisis stimulated research and development in to alternative forms of energy production, including wind power. The modern wind turbine that has emerged has two or three blades configured around a horizontal axis of rotation. The blades are attached to the nacelle, which houses the mechanical components, and is mounted on a tall tower [2]. Figure 1.1 is a photograph of a typical large wind turbine at Wolfe Island, Ontario.

In Canada, the adoption of wind power has increased dramatically over the past decade, as shown in Figure 1.2. As of March 31, 2011, there was 4,825 MW of installed wind turbine capacity across 133 wind farms [3]. The growth of the industry has been largely thanks to funding and initiatives from the federal and provincial governments, such as Canada's Wind Power Production Incentive introduced in 2002 [4], and Ontario's Feed-in Tariff (FIT) Program introduced in 2009 and based on previous Request for Proposals for renewable energy projects [5]. These programs were designed to help make renewable power production financially competitive with traditional power production, thus enabling and encouraging developers to build renewable projects.

Wind power is not viable everywhere, however. One of the first steps in developing a wind power project is to conduct a wind resource assessment (WRA). The purposes of a WRA are to investigate the characteristics of the wind, to identify and plan appropriate wind turbine installations, to evaluate the wind energy potential of said installations, and to determine the feasibility of the proposed project.

Figure 1.1: A Siemens 2.3 MW wind turbine installation at Wolfe Island, Ontario

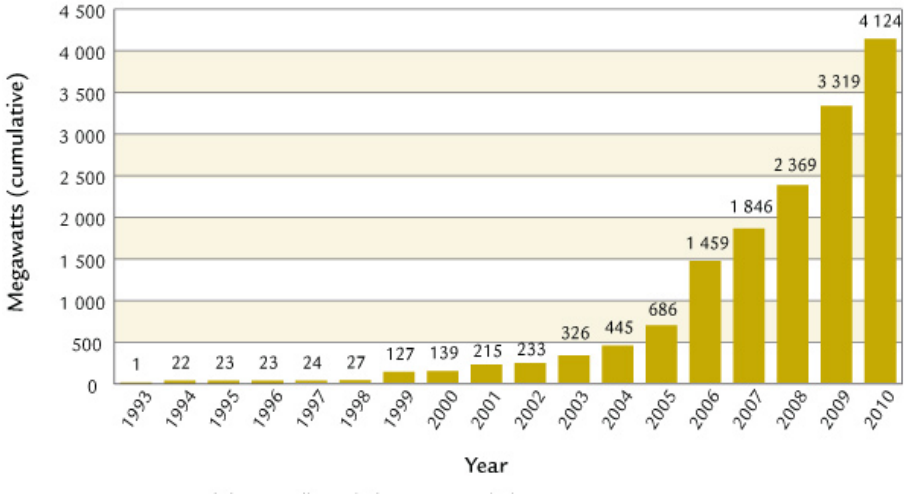

Figure 1.2: Canadian wind power cumulative capacity, 1993 to 2010 [3]

Chapter 2

Theory

2.1 Wind resource assessment

A wind resource assessment involves measuring and analyzing the wind speed and other meteorological data at a site. Some of the qualities that can be examined include the wind speed distribution, wind direction distribution, wind shear, and turbulence intensity. The most important quantity to estimate is the annual energy production of proposed wind turbine installations, which will determine the economic feasibility of the project. There are numerous methods for carrying out the various parts of a wind resource assessment. This study will cover the fundamental aspects of a wind resource assessment while comparing some of the possible methods, using meteorological data collected in the Waterloo region.

2.2 Wind speed distribution

The wind speed distribution at a site can typically be described by the Weibull probability density function given by Equation 2.1 [2, 6, 7].

$$f(x;\lambda,k) = \begin{cases} \frac{k}{\lambda}\left(\frac{x}{\lambda}\right)^{k-1} e^{(-x/\lambda)^k} & x \geq 0 \\ 0 & x < 0 \end{cases} \tag{2.1}$$

There are two parameters in the Weibull function; λ is the scale parameter and k is the shape parameter. x is the variable being measured, in this case wind speed. To estimate the Weibull parameters when given time-series wind speed data, the maximum likelihood method is recommended [8, 9]. The shape parameter k is solved by iteration and then the

scale parameter λ is solved explicitly, as given by Equations 2.2 and 2.3 respectively, where x_i is a measured data point and N is the size of the data set.

$$k = \left(\frac{\sum_{i=1}^{N} x_i^k \ln(x_i)}{\sum_{i=1}^{N} x_i^k} - \frac{\sum_{i=1}^{N} \ln(x_i)}{N} \right)^{-1} \tag{2.2}$$

$$\lambda = \left(\frac{\sum_{i=1}^{N} x_i^k}{N} \right)^{1/k} \tag{2.3}$$

At most sites, the shape parameter k is often around 2 [2], which is a good initial estimate to use for the iterative process. In fact, for the purposes of design calculations, the International Electrotechnical Commission (IEC) specifies the assumption of a Rayleigh distribution of wind speeds, which is equal to the Weibull distribution with a shape parameter of 2 [10]. Higher shape parameter is desirable, as it means stronger and steadier winds, as shown in Figure 2.1.

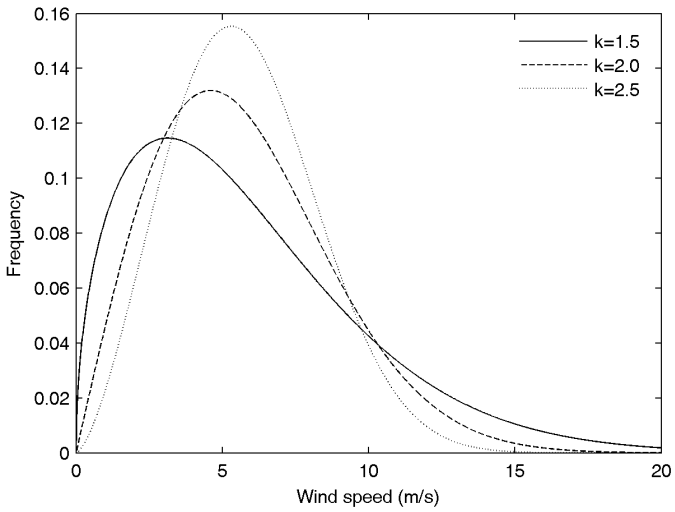

Figure 2.1: Weibull distributions with scale parameter (λ) 6.0 and varying shape parameters (k).

There are some alternatives to the Weibull distribution, such as a log-normal distribution [11, 12], a maximum entropy principle type function [13, 14], or a bimodal probability distribution where appropriate [15].

2.3 Wind speed variability

The wind speed distribution often varies with wind direction, height above ground, season, and time of day. The relationship between wind speed and wind direction is typically presented as a wind rose plot, which is simply a type of graph (such as a stacked histogram) of wind speed vs. wind direction in polar coordinates; for example, Figure 2.2. Ideally there will be one dominant wind direction with a small spread, but depending on the terrain and meteorology, other shapes may occur.

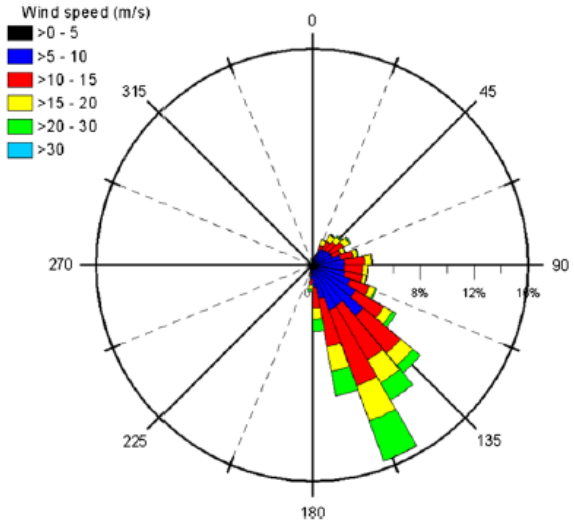

Figure 2.2: Wind rose at 50m in Triunfo, Brazil [16]

Wind tends to be stronger during the day than the night. At night, the temperature profile of the air is relatively stable, with colder, denser air near the surface and warmer air higher up. During the day, the sun warms the surface of the Earth, which disrupts the existing temperature stratification. Consequently, there is increased motion in the air due to convection. This is what drives the wind on a local scale, near the surface [6, 17].

Conversely, wind tends to be stronger during the winter than the summer in North America, Central America and the Caribbean. The prevailing winds are driven by the temperature and pressure difference between the equator and the poles, as air masses move from high pressure areas to low pressure areas. This temperature and pressure difference is greater during the winter, and so the motion of air is also greater. This is what drives the wind on a global scale [17, 6].

A wind resource study conducted in Grenada exhibited the diurnal and seasonal patterns described above [18], as shown in Figure 2.3.

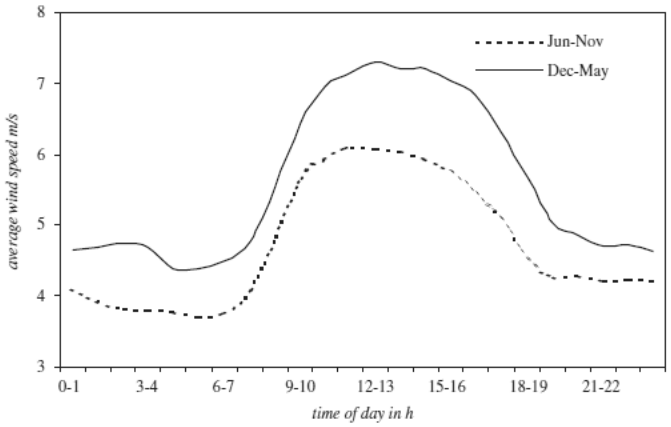

Figure 2.3: Diurnal and seasonal patterns of wind velocity, Grenada (1996) [18]

2.4 Wind shear profile

In fluid mechanics, a boundary layer is the layer of fluid on the surface of a body in a viscous flow. The atmospheric boundary layer (ABL) is the boundary layer on Earth's surface. The physical properties of air – such as velocity, temperature, and humidity – vary significantly in this layer [2]. The ABL height is generally between 100m to 2km above Earth's surface, and wind turbines certainly operate within this range [6].

A wind velocity profile exists in the ABL due to the aerodynamic drag over the surface and the viscosity of the air. At the surface, the wind speed is zero, and as height increases, the wind speed increases [2]. The velocity profile can be described by a power function or a logarithmic function, as in Equations 2.4 and 2.5 respectively.

$$\frac{U(z)}{U(z_{ref})} = \left(\frac{z}{z_{ref}}\right)^{\alpha} \tag{2.4}$$

$$\frac{U(z)}{U(z_{ref})} = \left(\frac{\log\left(z/z_0\right)}{\log\left(z_{ref}/z_0\right)}\right) \tag{2.5}$$

Where $U(z)$ is the wind speed at height z. z_{ref} is an arbitrary reference height. The shape of the power law profile is determined by α, the roughness exponent; and the shape of the log law profile is determined by z_0, the roughness length. Figure 2.4 [19] depicts both types of profiles.

Wind speed measurements may be unavailable at a proposed wind turbine's hub height, especially for large turbines. By measuring wind speeds at lower heights and applying a curve fit, wind speeds at higher heights can be extrapolated. For the purposes of energy calculations, typically only the wind speeds at hub height are used. However it is

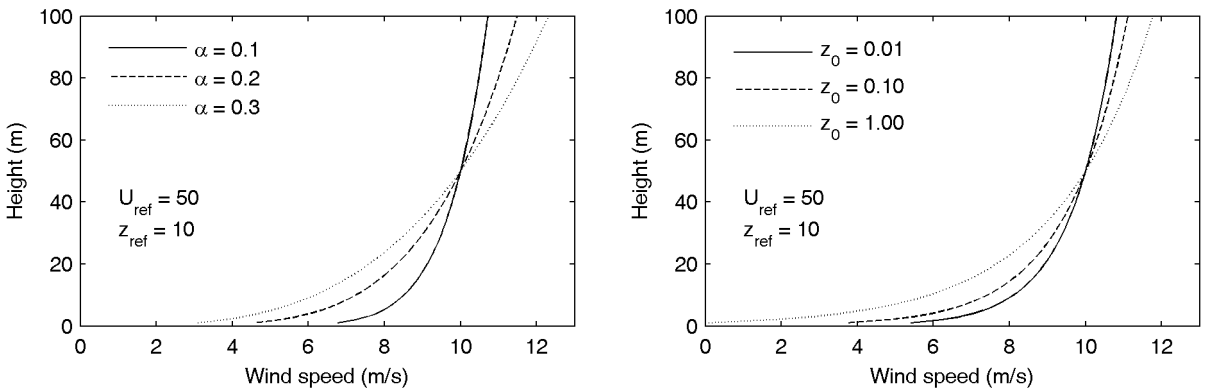

(a) Power law (b) Log law

Figure 2.4: Example wind shear profiles using power law and log law models.

important to consider the range of wind speeds passing through the rotor's swept area. It has been shown that the wind shear profile alters the performance of wind turbines [20, 21, 22], although in the context of a wind resource assessment, it is difficult to predict this adjustment.

Typical values for the roughness exponent in the power law model (α) and the roughness length in the log law model (z_0) are tabulated in Tables 2.1 and 2.2. These values were compiled by Ray, Rogers and McGowan [19] from results provided by many developers and researchers. The IEC specifies the assumption of a power law profile with exponent 0.2 for the purpose of design calculations [10]. Prandtl suggested a 1/7 power law for the velocity profile of turbulent flow over a flat plate, which would be an idealized scenario for the surface of the earth [23]. However, wind shear at a site is not a singular value, but is affected by a number of factors such as wind speed, wind direction, season, and time of day [24].

Terrain description	Roughness exponent α
Smooth, hard ground or sea	0.10
Short grass on untilled ground	0.14
Many trees and few buildings	0.22-0.24
Urban areas with tall buildings	0.4

Table 2.1: Typical roughness exponents for various types of terrain [19]

Terrain description	Roughness length z_0 (m)
Calm open sea	0.0002
Fallow field	0.03
Forest and woodlands	0.5
Suburbs	1.5

Table 2.2: Typical roughness lengths for various types of terrain [19]

One advantage of the power law model is that it can be linearized, therefore the curve fit can be solved explicitly. With the log law model, the curve fit must be computed with some type of iterative numerical method.

2.5 Wind shear power law model

Since the power law model can be linearized, a second parameter can easily be considered as well. In the one-parameter model given by Equation 2.6, the only unknown parameter is the roughness exponent α_{1p}, which sets the shape of the curve. The reference height z_{ref} and reference velocity $U(z_{ref})$ are arbitrarily fixed constants. The one-parameter curve will always pass through the reference height and velocity.

$$\frac{U(z)}{U(z_{ref})} = \left(\frac{z}{z_{ref}}\right)^{\alpha_{1p}} \tag{2.6}$$

A two-parameter model would be given by Equation 2.7, which has the roughness exponent α_{2p} and adds the new variable β. This means the curve is no longer constrained to intercept the reference height and reference velocity, although these values are still included in Equation 2.7 so that a comparison can be made to the one-parameter model.

$$\frac{U(z)}{U(z_{ref})} = \beta\left(\frac{z}{z_{ref}}\right)^{\alpha_{2p}} \tag{2.7}$$

Both the one-parameter and two-parameter models can be linearized, as shown in Equations 2.8 and 2.9.

$$\log\left(\frac{U(z)}{U(z_{ref})}\right) = \alpha_{1p}\log\left(\frac{z}{z_{ref}}\right) \tag{2.8}$$

$$\log\left(\frac{U(z)}{U(z_{ref})}\right) = \alpha_{2p}\log\left(\frac{z}{z_{ref}}\right) + \log\beta \tag{2.9}$$

The ordinary least squares (OLS) method is a well-known solution to the simple linear regression, and can be used to determine the two-parameter model parameters. A variant of OLS, the regression through the origin (RTO) method, can be used to determine the one-parameter model parameters. These methods are given by Equations 2.10 through 2.15. x_i and y_i are the independent and dependent variables respectively, and $\bar{x}$ and $\bar{y}$ are the means of those data sets. N is the number of points in the data set.

The root mean square error (RMSE) should be used to evaluate goodness-of-fit because it has a consistent definition in both OLS and RTO procedures. The coefficient of determination or R-squared value is calculated differently in OLS and RTO [25].

$$y_i = \log\left(\frac{U(z_i)}{U(z_{ref})}\right) \tag{2.10}$$

$$x_i = \log\left(\frac{z_i}{z_{ref}}\right) \tag{2.11}$$

$$\alpha_{1p} = \frac{\sum x_i \cdot y_i}{\sum x_i^2} \tag{2.12}$$

$$\alpha_{2p} = \frac{\sum (x_i - \bar{x}) \cdot (y_i - \bar{y})}{\sum (x_i - \bar{x})^2} \tag{2.13}$$

$$\log\beta = \bar{y} - \alpha_{2p} \cdot \bar{x} \tag{2.14}$$

$$RMSE = \sqrt{\frac{\sum (y_i - \hat{y}_i)^2}{N}} \tag{2.15}$$

The added computational complexity is insignificant, yet the results could potentially be better. In theory, the two-parameter model should always be able to match or perform better than the one-parameter model in terms of goodness-of-fit. If the roughness exponents are the same and $\beta = 1$, then the two models will be equal. Since the two-parameter model has greater flexibility, it should potentially fit better. Other linear regression procedures could yield even better results.

2.6 Turbulence intensity

Turbulence intensity (I_u) is a simple way to describe the degree of fluctuation in wind speeds. It is defined as the ratio of the standard deviation over the mean of wind speeds measured during a period of time.

$$I_u = \frac{\sigma_u}{\bar{U}} \tag{2.16}$$

Where σ_u is the standard deviation and $\bar{U}$ is the mean wind speed. Just as with wind shear, turbulence intensity can be affected by a number of factors, such as wind speed, wind direction, height above ground, season, and time of day [26, 24]. For the purposes of design calculations, the IEC specifications include a model of turbulence intensity as a function of wind speed, given by Equation 2.17 [10].

$$I_u = I_{15}\left(\frac{a + \frac{15}{\bar{U}}}{a+1}\right) \tag{2.17}$$

The parameters of the formula, I_{15} and a, depend on the target wind turbine class. Class A is a high turbulence model, and class B is a low turbulence model, as seen in Figure 2.5. Further explanation is provided in Section 2.7.

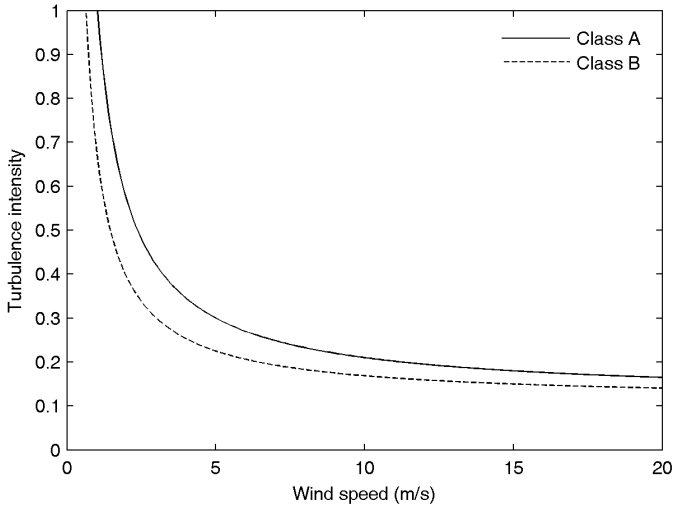

Figure 2.5: IEC design turbulence intensities for two wind turbine classes.

2.7 Wind turbine class

The IEC suggests several wind turbine classes based on the turbine's design mean wind speed and turbulence intensity. The specifications for each wind turbine class are listed in Table 2.3. I_{15} and a are parameters of the turbulence intensity model described in Section 2.6. The specifications also include formulas for 1-year and 50-year extreme wind speeds that the turbine should survive [10].

Class	I	II	III	IV
Mean wind speed (m/s)	10	8.5	7.5	6
1-year extreme (m/s)	52.5	44.6	39.4	31.5
50-year extreme (m/s)	70	59.5	52.5	42

Class	A (high)	B (low)
I_{15}	0.18	0.16
a	2	3

Table 2.3: IEC 61400-1 design wind speeds and turbulence intensity at hub height [10]

For example, the Siemens SWT-2.3-82 VS is a class IA turbine, which means it is designed for high winds and high turbulence intensity [27]. When selecting a wind turbine for a proposed installation, its class should be appropriate for the site.

2.8 Wind turbine power curve

The power curve of a wind turbine is its power output as a function of the wind speed. The power output largely depends on the wind speed, but is also affected by wind shear, turbulence intensity, off-axis wind direction, physical blade degradation, and other factors. Theoretically, the power (P) available in a volume of air of a certain density (ρ) moving at a constant velocity through a wind turbine's swept area (A) is cubically proportional to its speed (U), as given in equation 2.18. Therefore, wind speed is the most important factor in a wind turbine's performance.

$$P = \tfrac{1}{2}\rho A U^3 \tag{2.18}$$

An example of a wind turbine power curve is shown in Figure 2.6. The power curve is obtained with procedures and under conditions (ie: with respect to wind shear, turbulence intensity) described in the IEC standards [28].

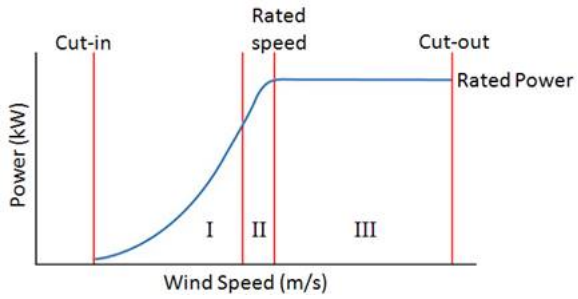

Figure 2.6: Example wind turbine power curve [29]

Below the cut-in wind speed the turbine will not operate, because there is not enough torque to rotate the blades or enough energy in the wind for feasible generation. As the turbine starts up, the power curve ramps up almost cubically, since the theoretical power available increases cubically with wind speed. Eventually the rotor is intentionally slowed and the power output is capped for mechanical and structural reasons. The generator's capacity coincides with this limit. This point it reaches the maximum is the turbine's rated wind speed and rated power. Above an even higher wind speed, the cut-out wind speed, the turbine will shut down to prevent structural damage from the heavy loads [29].

Unless otherwise stated, the power curve is assumed to be for the standard air density of 1.225 kg/m^3 [10]. According to Equation 2.18, power is proportional to density, so energy estimates should be adjusted accordingly. Knowing the atmospheric pressure (p), temperature (T), and relative humidity, the actual density of air (ρ) can be calculated. Assuming dry air, the ideal gas law can be used, given by Equation 2.19. The gas constant R is 287 J/kg.K for dry air [30].

$$p = \rho R T \tag{2.19}$$

2.9 Annual energy production

One of the main goals of a wind resource assessment is to calculate the annual energy production (AEP) of a proposed project, which will ultimately determine whether the project is financially viable. The AEP is calculated using the power curve and wind speed data.

Energy is simply the product of power and time. With measurements of wind speed over time ($U(t)$), and with the curve of power output vs. wind speed ($P(U)$), the numerical integral of power over time can be calculated to determine the amount of energy generated (E) by a proposed wind turbine installation [31].

Using continuous data, the formula can be written as:

$$E = \int_0^T P(U(t))\,\mathrm{d}t \tag{2.20}$$

Using discrete data, this is evaluated as:

$$E = \sum_{i=1}^{N} P(U(t_i))\Delta t \tag{2.21}$$

With a large set of data or with modelled data, this approach may be unfeasible. The method commonly used in industry is to sort the wind speed data into a histogram, multiply the frequencies ($f(U)$) by the power curve ($P(U)$) at each bin centre, and then sum over all the bins [31].

Using a continuous distribution, the formula can be written as:

$$E = T \int_0^{U_{max}} P(U) f(U)\,\mathrm{d}U \tag{2.22}$$

Using a discrete histogram, this is evaluated as:

$$E = T \sum_{i=1}^{N} P(U_i) f(U_i) \Delta U \tag{2.23}$$

Alternatively, a Weibull probability distribution can be used in place of the actual wind speed distribution in the above set of equations [7, 32]. This approach is less common but still used in some cases. For example RETScreen, a renewable energy technology project analysis software developed by Natural Resources Canada's CanmetENERGY research centre, predicts annual energy production based on the site's Weibull shape parameter and monthly mean wind speeds [33].

2.10 Capacity factor

The capacity factor of a power plant is the ratio of the actual annual energy production to the maximum possible energy production if it operates at its full nameplate capacity,

as shown in Equation 2.24. For wind farms, the range of values is generally from 20% to 40%, and over 30% is generally the target [34]. A low capacity factor may indicate that the wind resource is not good, or that the turbine is oversized.

$$\text{Capacity factor} = \frac{\text{Actual energy production}}{\text{Maximum possible energy production}} \tag{2.24}$$

2.11 Measure-Correlate-Predict

The wind speed distribution at a site varies from year to year, therefore it is important to take measurements for multiple years at the target site. However, the measurement campaign at the target site is usually limited by the project timeline. This can be ameliorated by incorporating wind speed data from another source that covers a longer period of time, such as a weather station. The long-term data can be used as a reference to extend the site data in a procedure called Measure-Correlate-Predict (MCP) [35].

The first step is to measure wind speeds for a short-term period at the target site, and obtain long-term data from a nearby reference site. There needs to be some overlap between the two measurement periods. If the reference site and target site are reasonably proximate, there should be a correlation in wind speeds between them during the concurrent measurement period. By applying this correlation to the long-term wind speed data at the reference site, the long-term wind speed distribution at the target site can be predicted. This distribution can lead to a better estimation of the AEP [35].

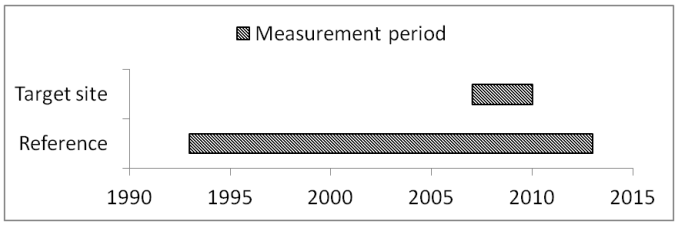

Figure 2.7: Illustration of the MCP method

There are various MCP algorithms that have been designed and used, the most basic of which involve mapping a linear relationship between concurrent wind speeds at the reference site and target sites. The common form of a linear equation is given by Equation 2.25.

$$y = mx + b \tag{2.25}$$

Where x is the independent variable, y is the dependent variable, m is the slope parameter, and b is the intercept parameter. In this case, x is the wind speed at the reference site, and y is the wind speed at the target site. The simplest way to solve for the slope and intercept is with the ordinary least squares (OLS) method, which has an analytic solution [36] given by the Equations 2.26 through 2.30. x_i and y_i are the independent and dependent variables respectively, and $\bar{x}$ and $\bar{y}$ are the means of those data sets.

$$S_{xx} = \sum (x_i - \bar{x})^2 \tag{2.26}$$

$$S_{yy} = \sum (y_i - \bar{y})^2 \tag{2.27}$$

$$S_{xy} = \sum (x_i - \bar{x})(y_i - \bar{y}) \tag{2.28}$$

$$m = S_{xy}/S_{xx} \tag{2.29}$$

$$b = \bar{y} - m\bar{x} \tag{2.30}$$

The correlation coefficient, a measure of the goodness-of-fit with the OLS method, is given by Equation 2.31.

$$R^2 = \frac{S_{xy}^2}{S_{xx}S_{yy}} \tag{2.31}$$

There are some issues with the OLS regression. It involves assumptions that are questionable, such as that the relationship is inherently linear, and that the errors are independent (which is very inaccurate given that this is time series data). Also, the mean and variance in the predicted $\hat{y}$ values will not be the same as the mean and variance in the measured y values during the concurrent measurement period. This causes the wind speed distribution at the target site to become altered after applying the regression [37]. Because of these weaknesses, the OLS method should only be considered a baseline on which other methods should improve.

To address the last issue mentioned above, Rogers et al. [37] proposed the "variance ratio" method of linear regression. It is very similar, but the slope is taken to be the ratio of the standard deviation of the reference site and the target site wind speeds, as shown in Equation 2.32. The goodness-of-fit is reduced, but this ensures the mean and variance of the wind speed distribution at the target site during the concurrent measurement period remain unchanged.

$$m = \sqrt{S_{yy}/S_{xx}} \tag{2.32}$$

Optionally, low wind speed data may be omitted, or the data can first be sorted into wind direction bins and regressions can be calculated for each bin [2]. Some alternative MCP algorithms include using a power law regression [38], a two-dimensional linear regression [37], or a joint probabilistic approach [39]. Only the two methods described above will be explored, since a meaningful comparison between these methods can be made with the data available.

For this project, three potential long-term weather stations were identified for MCP analysis: at WRESTRC (the same site as the met tower), at the University of Waterloo [40], and at the Region of Waterloo International Airport [41]. These are the three nearest sources of wind speed and wind direction data that could be found. They cover different date ranges and record in different intervals. Table 2.4 lists these characteristics.

Weather station	WRESTRC	University	Airport
Years (inclusive)	2004-2010	1999-2010	2003-2009
Recording interval	1 hour	15 mins	1 hour
Distance from WRESTRC (km)	<0.5	4.5	15.0
Distance from RIM Park (km)	11.5	7.0	10.5

Table 2.4: Reference weather stations in the Waterloo region

2.12 Uncertainty analysis

Just as the wind speed distribution varies year-to-year, the AEP will vary year-to-year. It is customary to report two values: the AEP that has a 50% chance of being exceeded (P50), and the AEP that has a 90% chance of being exceeded (P90), assuming a Gaussian probability distribution. The ratio P90/P50 is useful in comparing different prospective wind farm projects [42].

The central estimate (P50) is the mean AEP calculated above with systematic uncertainties factored in, such as the ones listed in Table 2.5. These are generally sources of energy loss.

The outer estimate (P90) is related to the statistical uncertainties in calculating the mean AEP, such as the ones listed in Table 2.6.

Energy loss factor	Description
Electrical efficiency	Losses in electrical transmission from turbine to battery, substation, or other endpoint.
Availability	Losses due to shutdown for external reasons, such as maintenance, grid down-time, etc.
High wind speed hysteresis	A turbine shuts down when the wind speed increases above the cut-off, but does not start up again until the wind speed decreases well below the cut-off.
Icing and blade degradation	Changes to the blade profile due to ice accumulation and surface degradation decrease in the power performance of the turbine.

Table 2.5: Sources of uncertainty in the central estimate [43, 44]

Some of the sources of uncertainty are outside the scope of this study, as they can't be accounted for without further information.

Lackner et al. [44] outline a deterministic procedure for calculating the AEP uncertainty when using a Weibull distribution. Kwon [31] presents a numerical procedure that employs the Monte Carlo simulation method. Without going to the same extent as either of these procedures, an estimate of the uncertainties in AEP can be developed by following the same mathematical guidelines.

To start, the uncertainty in the mean of a data set ($\delta\mu$) is not simply the standard deviation (σ), but that value divided by the square root of the number of samples (N):

$$\delta\mu = \sigma/\sqrt{N} \tag{2.33}$$

IEC standards on power performance measurement of wind turbines define a way to report the uncertainty of cup anemometers as a function of the wind speed reading. It is given by equation 2.34.

$$\delta U = (0.05 + 0.005U)K/\sqrt{3} \tag{2.34}$$

Where K is a classification number provided by the manufacturer, and is based on standardized testing of the anemometer. For the NRG #40C anemometer, $K = 2.4$ under

Source of uncertainty	Description
Wind speed measurement	Uncertainty due to anemometer calibration, tower effects, data reduction, etc.
Long-term estimation	MCP correlation uncertainty and long-term wind speed distribution uncertainty
Wind speed variability	Only a finite number of years are used; true variability will be greater
Wind speed transformation	Uncertainty due to wind shear extrapolation and wind flow modelling
Power curve adjustment	IEC specifies standard conditions for power curve measurement; site conditions are different

Table 2.6: Sources of uncertainty in the outer estimate [43, 44]

class A type wind flow (ideal flat terrain, low turbulence) and $K = 7.7$ under class B type wind flow (complex terrain, high turbulence).

Multiple sources of uncertainty can be combined, assuming they are independent and normally distributed, by the standard formula, Equation 2.35.

$$\delta f = \sqrt{\sum_{i=1}^{N} \left(\frac{\partial f}{\partial x_i} \delta x_i \right)^2} \tag{2.35}$$

Where f is a linear combination of multiple variables, x_i. The assumptions used may not be accurate, but are necessary simplifications [43, 44].

Chapter 3

Data collection

3.1 W3 Wind Energy Project

In 2007 the City of Waterloo, in partnership with the Region of Waterloo and University of Waterloo, was granted $55,000 from the Federation of Canadian Municipalities (FCM) to conduct a wind energy feasibility study and implement a demonstration site. The funds were matched by the City and the Region. The motivation behind this project was to explore the possibility of wind power in the area, and to raise awareness for wind power in the community. The steering committee was comprised of City of Waterloo staff, Region of Waterloo staff, and University of Waterloo faculty and students. In 2008, two 50m tall meteorological (met) towers were installed at two locations in order to measure the wind and weather characteristics at those sites. With the measurement data, a feasibility study was performed. In 2011, a project report was submitted to FCM detailing the study approach, relevant government policy, community engagement activities, wind resource measurements and analysis, and recommendations towards implementing a wind power demonstration site [45].

3.2 Measurement locations

Two measurement locations were selected near the boundaries of the Waterloo area. Of the land available to the Region and City of Waterloo, these two sites were deemed most appropriate for wind power based on the terrain [45]. The locations are the Waterloo Region Emergency Services Training and Research Complex (WRESTRC), which is west of the city; and the RIM Park recreational area, which is northeast of the city. The WRESTRC tower is closely surrounded by small buildings and trees to the east, while the RIM Park tower, pictured in Figure 3.1, is in a slight valley in an open area. Neither location seemed

suitable for commercial wind farms, but there were no better sites available, and small wind turbines are often placed in similarly rough terrain. The towers are labeled as red dots in the aerial photographs in Figure 3.2. The scale bar is 1km.

Figure 3.1: The met tower at RIM Park

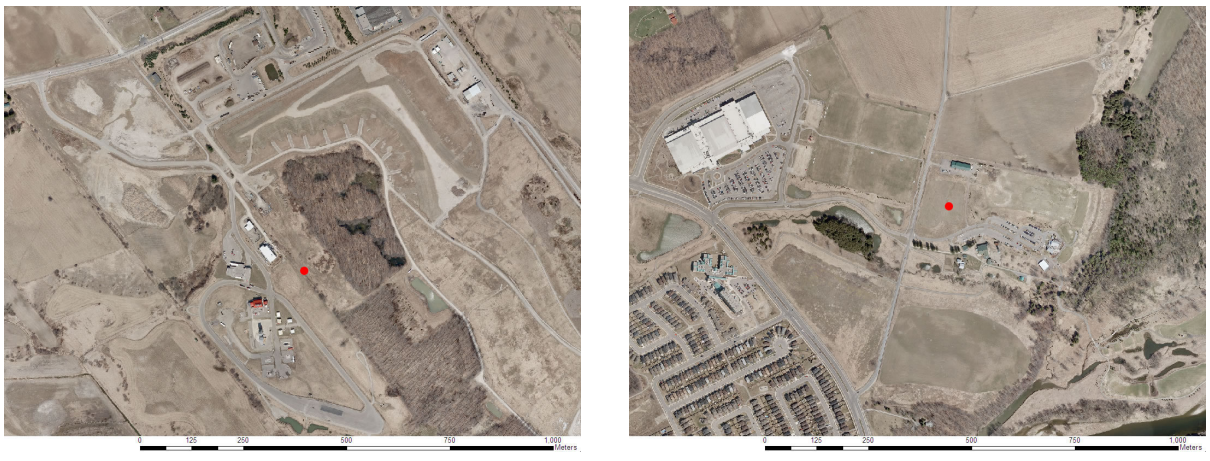

(a) WRESTRC (b) RIM Park

Figure 3.2: Aerial photographs of the met tower locations [46]

3.3 Towers and equipment

Two complete packages – which include the tower, booms, sensors, and data logger – were purchased from NRG Systems (NRG) [47], and additional sensors were purchased from R.M. Young (RMY) [48]. These instruments were chosen because both companies' equipment are commonly used in industry, and conform to the IEC 61400-12 wind turbine power performance testing standard [28]. Images of each sensor are shown in Figure 3.3.

(a) NRG #40C anemometer (b) NRG #200P wind vane (c) RM Young wind monitor

(d) NRG #110S temperature sensor with radiation shield (e) NRG #BP20 barometric pressure sensor

Figure 3.3: Meteorological instruments [47, 48]

The NRG anemometer is a cup-type anemometer, which consists of a coil surrounded by a four pole magnet. Rotation of the coil induces a sine wave voltage with frequency up to 125 Hz. The NRG wind vane essentially consists of a rotational potentiometer with a tail fin that naturally orients the sensor in the prevailing wind direction. The RMY anemometer is a propeller-type anemometer that can measure both wind speed and wind direction simultaneously. The NRG temperature and pressure sensors use integrated circuits to measure the absolute temperature and pressure.

Both towers had five NRG anemometers, one NRG wind vane, one RMY anemometer, one temperature sensor, and one pressure sensor. Multiple anemometers were placed at different heights, because wind speed varies with height, especially in the ground level

to 50m range. There were redundant anemometers at the higher locations to improve reliability and data capture rate. Temperature and pressure are less sensitive to height, therefore those sensors were placed near the ground. The layout of the sensors is listed in Table 3.1. Further details of the setup is available in Appendix A.

Height (m)	Instruments
1	NRG #110S temperature sensor, NRG #BP20 pressure sensor
20	NRG #40C anemometer
30	NRG #40C anemometer, NRG #200P wind vane
40	NRG #40C anemometer, NRG #40C anemometer
50	NRG #40C anemometer, RMY wind monitor 05103

Table 3.1: Instrument locations on the met tower [45]

The met towers were equipped with NRG Symphonie data loggers, which sample the sensors every 2 seconds, and record mean, maximum, minimum, and standard deviation values in 10 minute intervals. Data was stored on a removable MultiMediaCard (MMC). Each logger was equipped with a GSM iPack and SIM card, which allowed it to send data daily over the GSM cellular network to multiple email addresses. The loggers were powered by D-cell batteries, and the iPacks were powered by small 5W solar photovoltaic panels and 12V batteries [49].

The logger had six counter channels (occupied by the six anemometers) and six analog channels (occupied by two wind vanes, the temperature sensor, pressure sensor, and battery voltmeter). It read AC signals from the counter channels and can measure frequencies up to 2500 Hz. It read DC signals from the analog channels with a 10-bit A/D converter; full-scale range was zero to the excitation voltage. Signal conditioning modules (SCM) were purchased for each instrument, which fit into the data logger and automatically configured it to properly read the instruments. The calibration curves and measurement ranges are listed Appendix A. The NRG anemometers were purchased pre-calibrated; each had an individual calibration curve, which were all similar to the general curve. The RMY anemometer could survive gusts up to 100 m/s, though it was not effective beyond 60 m/s. The wind vanes, which work as potentiometers, all had a dead zone between 355°and 360°[49, 50].

3.4 Anemometer calibration

Before being installed on the met towers, the NRG and RMY anemometers were tested in a 61cm by 61cm open jet wind tunnel, using a Pitot-tube to provide the reference velocity. The Pitot-tube and pressure transducer were calibrated with an inclined water manometer. After one of the met towers was decommissioned in 2011, the NRG anemometers were tested again in the same wind tunnel, but with an unopened and unused NRG anemometer to provide the reference velocity.

A rotational anemometer essentially consists of a coil surrounded by magnets. As the coil rotates, a sine wave voltage is induced through it. The frequency of the sine wave is related to the frequency of rotation (and the number of poles), which is related to the flow speed. Therefore the calibration curve is of flow speed (m/s) vs frequency (Hz).

In the first set of tests, the flow speeds reported by the Pitot-tube follow a line with higher offset and lower slope than the manufacturers' calibration curves, especially for the RMY anemometer. This systematic error is probably attributed to the imperfect calibration of the Pitot-tube.

In the second set of tests, the flow speeds reported by the used NRG anemometers matched very well with the unused anemometer. These results suggest that two years of operation did not affect the calibration of the instruments.

Ultimately, the manufacturers' calibration curves were applied to the data for all the instruments, regardless of the results of these experiments. It was decided that the manufacturers' testing was likely more reliable than our own.

3.5 Tower shadow

After the meteorological data has been collected, inaccurate or unreliable measurements need to be detected and filtered. Two of the possible causes of unusable data are tower shadow and icing.

The presence of the tower affects the local flow field. Generally the flow slows down in front of the tower, accelerates around it, and then breaks down into a wake behind it. The IEC 61400-12-1 guidelines recommend placing two anemometers at the same height, upstream of the tower, at 45°from the dominant wind direction, as this is where the flow disturbance is minimal [28].

The flow disturbance is most pronounced in the wake of the tower, where studies have shown there is a significant velocity deficit due to presence of the tower. It is clearly visible when comparing the wind speed ratio between two anemometers at the same height [51, 52, 53].

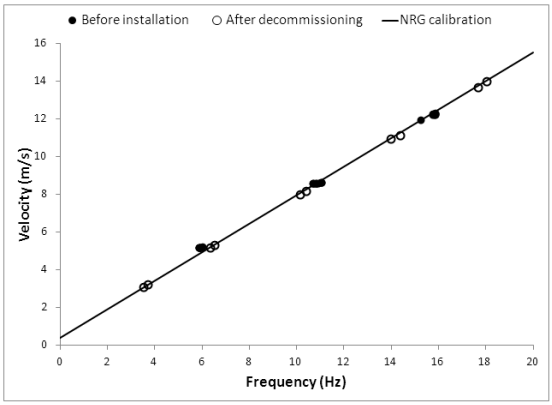

(a) NRG anem. 69485

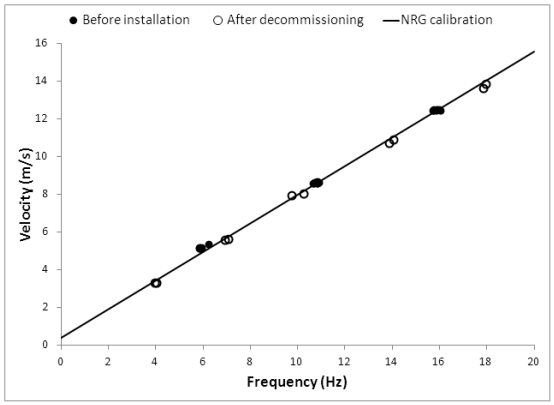

(b) NRG anem. 69589

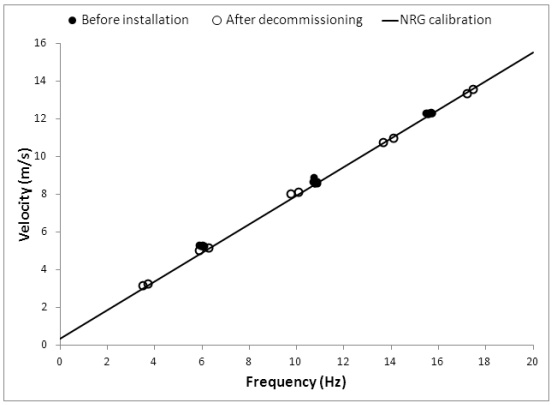

(c) NRG anem. 69651

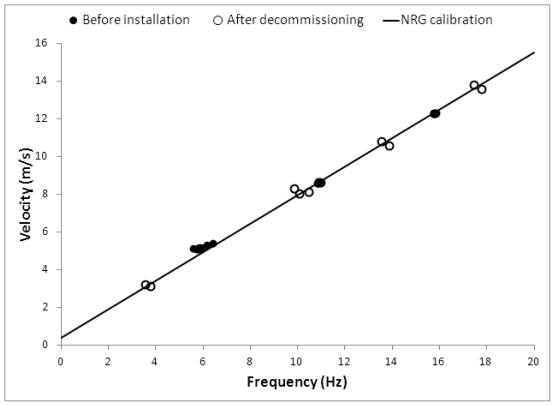

(d) NRG anem. 69655

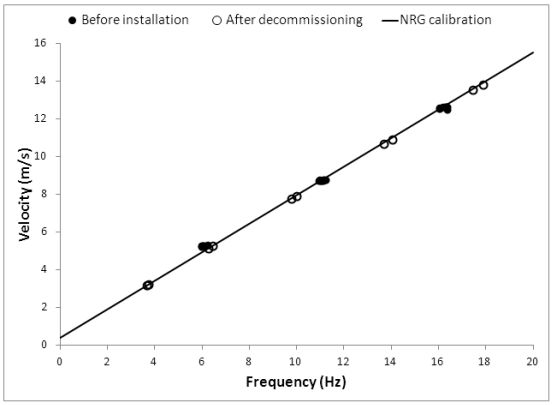

(e) NRG anem. 70294

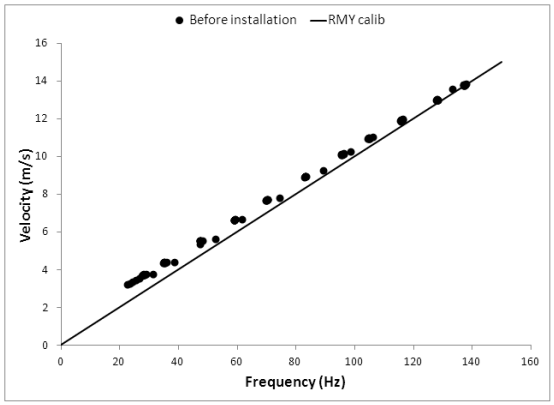

(f) RMY anem. 88324

Figure 3.4: Wind tunnel tests of manufacturer calibration curves.

Where there are multiple anemometers at the same height, data can be selected to avoid the tower shadow effect. At both WRESTRC and RIM Park, there were visible velocity deficits when the wind direction is around 300°(northwest wind), while the velocity peaks at around 90°at WRESTRC and 160°at RIM Park are less pronounced. A deficit indicates when one anemometer is in the tower shadow, and a peak indicates when the other anemometer is in the tower shadow. The difference in severity between the deficits and the peaks can be attributed to the fact that the dominant wind direction at both sites is from the northwest, so there are more data points in that range, and wind speeds are quite low outside that range.

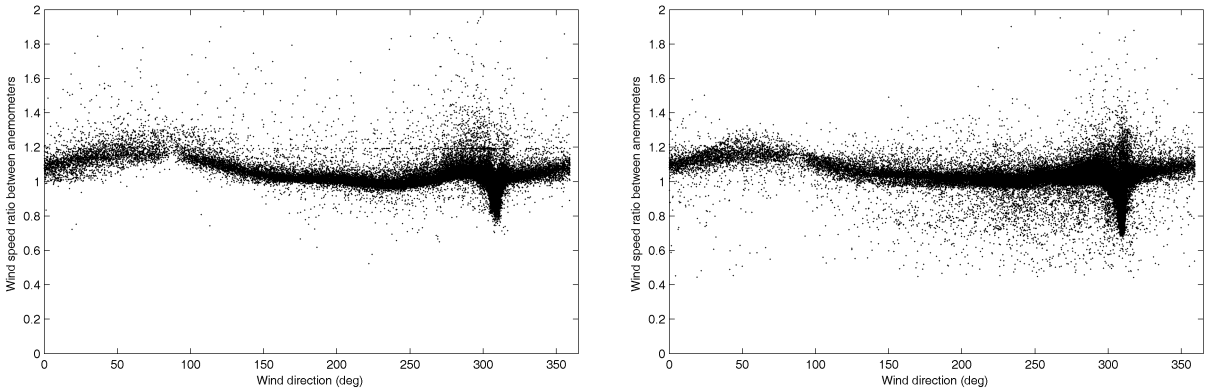

(a) 40m (b) 50m

Figure 3.5: Effect of tower shadow on wind speed measurement at WRESTRC.

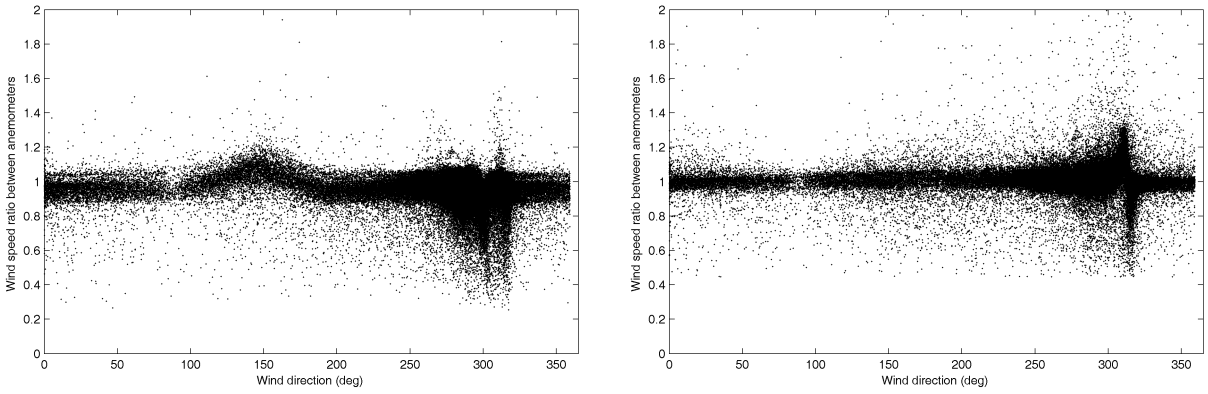

(a) 40m (b) 50m

Figure 3.6: Effect of tower shadow on wind speed measurement at RIM Park.

3.6 Icing

Wind vanes and anemometers, particularly the cup-type ones, are vulnerable to icing in the winter, which causes inaccurate and unusable data. Icing events are typically marked by abnormal spikes in standard deviation values, accompanied by temperatures below freezing and high relative humidity. If the ice continues to build up, the vanes and anemometers will completely freeze and the mean and standard deviation values will drop to zero [54].

Icing events are difficult to detect in post-processing without an icing sensor or a heated anemometer for comparison. But if conditions worsen to the point that the instruments freeze, these events are easy to identify because the instrument output will be fully suspended. Figure 3.7 is an example that illustrates both the NRG anemometer and wind vane freezing. The temperature stays just below zero while a low pressure area moves in, suggesting a weather event such as snow or freezing rain.

The NRG and RMY anemometers and vanes correlate strongly in good weather, but their outputs are quite different in bad weather. At the start of the icing event, the NRG anemometer reported higher wind speeds than the RMY anemometer for several hours. The explanation for the overspeeding is that cup-type anemometers are inertia-based, and a small amount of ice accumulation on the cup can cause it to rotate faster and to continue rotating quickly even as wind speeds drop. This typically occurs during highly turbulent flows when a gust can drive rotation for long after it passes [55]. Eventually the NRG anemometer completely stopped for roughly 24 hours. But the RMY anemometer continued to operate, likely because it is a propeller-type anemometer, which can deflect ice and snow buildup to some extent. At roughly the same time, the NRG vane stopped completely, while the RMY vane appeared to become "sticky"; in other words, it became less responsive and less reliable due to ice/snow around its base.

After the weather improved, the instruments began to rotate again, but it took more than a day to thaw out. During the thawing process, the NRG anemometer tended to report lower wind speeds than the RMY anemometer. This is likely because the added mass from the ice/snow made it more difficult to rotate the cups. Eventually the anemometers and vanes returned to their normal state, where the correlation between the sensors is strong.

3.7 Data filtering

Parent and Ilinca [56] recommend using a dedicated icing sensor, a heated anemometer, or temperature and relative humidity sensors to detect icing events during the site assessment phase. However, the Waterloo met towers were not properly equipped for any of these techniques. With only anemometer data, Kenyon and Blittersdorf [54] suggest excessively high or low standard deviations are evidence of icing, but this did not seem to be true

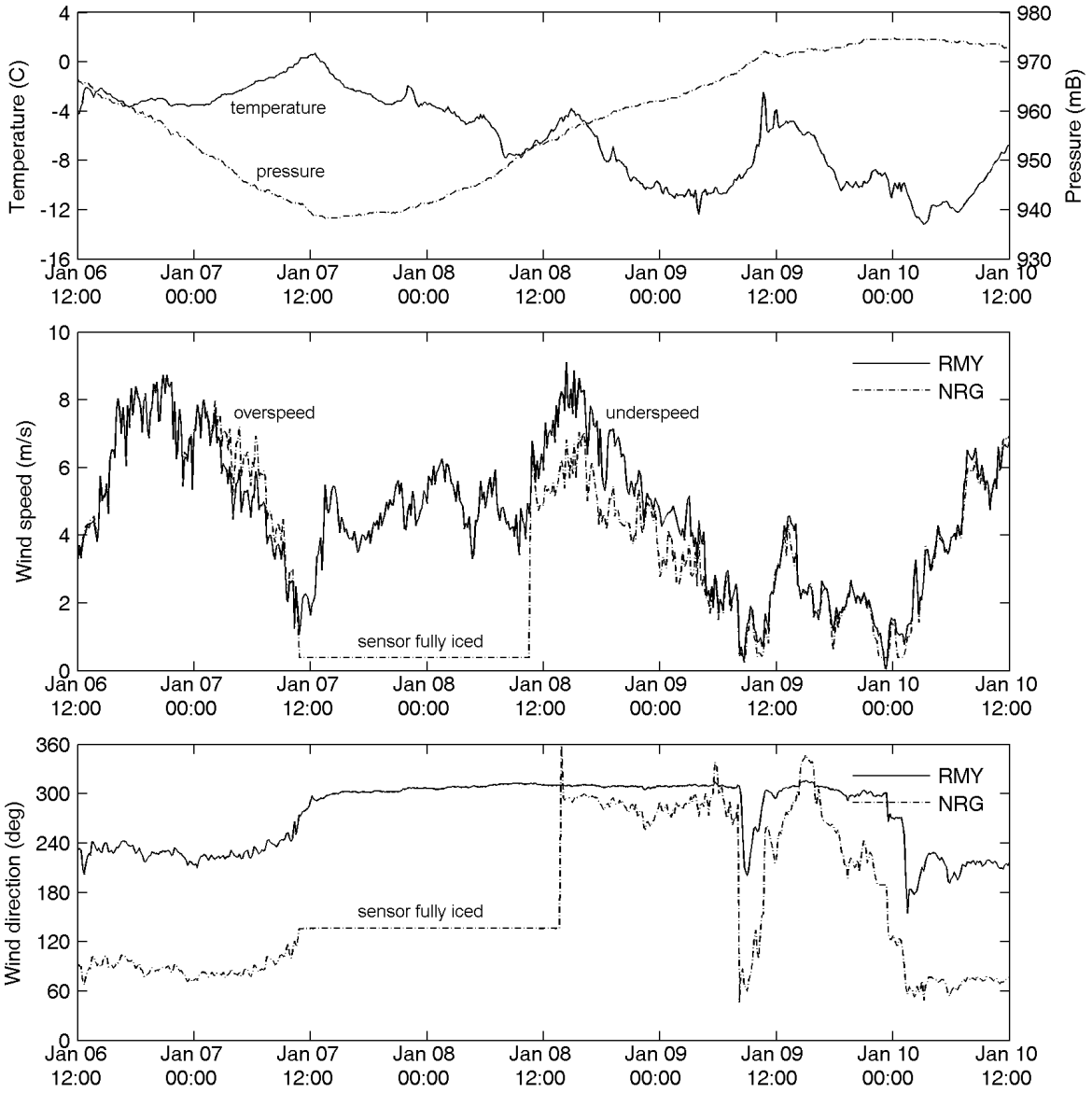

Figure 3.7: Temperature, pressure, wind speed and wind direction measurements during a weather event at WRESTRC in 2009

for all icing events such as the one noted above at WRESTRC. Ultimately the double anemometry method in Parent and Ilinca was used, in which an icing event is assumed when the difference between the wind speeds measured by heated and unheated anemometers exceeds a certain limit.

In the absence of a heated anemometer, the RMY anemometer was chosen as the reference since it seemed to be the most reliable. The conditions for rejection were created empirically, by observing the scatter graphs of wind speeds between the RMY anemometer and other anemometers' wind speeds. In the scatter graphs in Figure 3.8, there are obvious areas of overspeed and underspeed, and areas where sensors are completely unresponsive. The data filtering process was designed to remove these data points.

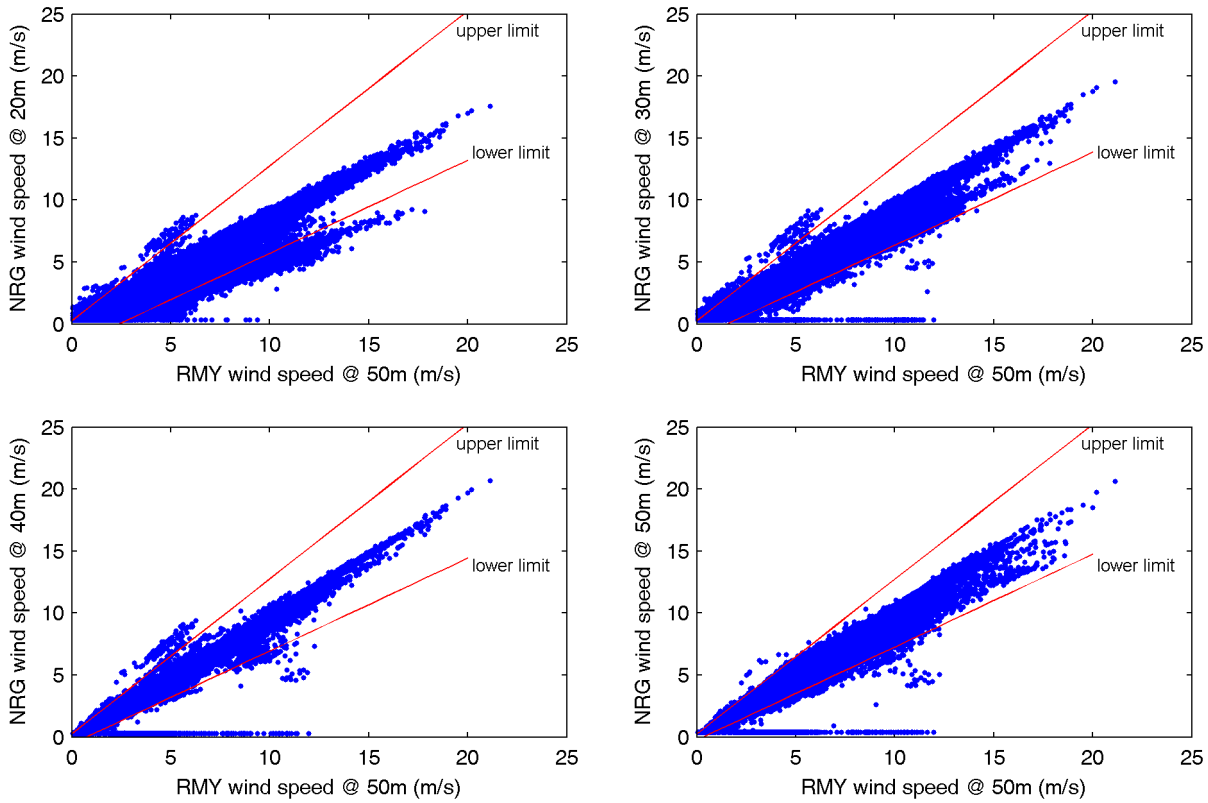

Figure 3.8: Scatter of NRG anemometers vs RMY anemometer at WRESTRC, with data filtering limits.

The upper and lower limits of the acceptable range are given in Equations 3.1 and 3.2 respectively.

$$U_{limit,upper} = U_{ref} + (U_{ref} + 1)/4 + \begin{cases} d & \text{if } d > 0 \\ 0 & \text{if } d < 0 \end{cases} \tag{3.1}$$

$$U_{limit,lower} = U_{ref} - (U_{ref} + 1)/4 + \begin{cases} 0 & \text{if } d > 0 \\ d & \text{if } d < 0 \end{cases} \tag{3.2}$$

Where d is mean difference of wind speeds between two anemometers (eg: on average, the wind speed at 20m is 1.5 m/s lower than the wind speed at 50m). Ideally the correlation between two anemometers at the same height should follow the line $y = x$. The second term in the above equations allows for greater variation at higher wind speeds. The third term accounts for difference in mean wind speeds by offsetting either the upper or lower limit, depending on if the difference is positive or negative.

The percentage of accepted data by each anemometer is listed in Table 3.2. Overall the data capture rate is very high except for two anemometers: the 20m one at WRESTRC and the 30m one at RIM Park. There did not appear to be any problems with the calibration of either sensor, but they experienced greater difficulties with icing, possibly due to positioning or manufacturing discrepancies.

WRESTRC			RIM Park		
Sensor	Height (m)	Capture rate	Sensor	Height (m)	Capture rate
70307	20	93.2	69651	20	97.2
69592	30	98.9	69589	30	92.9
69464	40	99.1	69655	40	99.3
70249	40	99.3	69485	40	99.1
69659	50	98.7	70294	50	99.1

Table 3.2: Data capture rate after filters applied.

Chapter 4

Results and discussion

Measurements of wind speed, wind direction, temperature and pressure were recorded for over two years at two sites in the Waterloo region: WRESTRC and RIM Park. This data was used to characterize the wind resource and to assess the feasibility of wind power at the sites.

4.1 Wind turbine class

The mean and maximum wind speeds recorded are summarized in Table 4.1. Comparing these results to the definitions in Table 2.3, an IEC Class IV turbine is recommended, since the mean and maximum wind speeds match this class best. Class IV turbines are typically small wind turbines under 50kW in capacity and under 50m in height. WRESTRC is likely a more viable site for a wind turbine than RIM Park, since its mean wind speeds are greater. As expected, wind speed increases with height from the ground, and the increase is larger at WRESTRC than at RIM Park. Further analysis on wind shear is discussed in section 4.5.

4.2 Wind speed distribution

The wind speed histograms at each height and at both sites are shown in Figures 4.1 and 4.2. In addition, the Weibull function, explained in Section 2.2, was fitted to the wind speed distributions, and the scale (λ) and shape (k) parameters are tabulated in Table 4.2.

The Weibull distribution may in general be a good representation of average wind speeds at most locations, but it does not fit either of these Waterloo sites well. In all cases,

	WRESTRC		RIM Park	
Height (m)	Mean (m/s)	Max (m/s)	Mean (m/s)	Max (m/s)
20	4.00	29.5	3.82	25.4
30	4.61	30.6	4.16	27.3
40	5.20	30.7	4.39	29.9
50	5.49	31.1	4.67	30.3

Table 4.1: Wind speed statistics collected during the years 2009 and 2010.

	WRESTRC		RIM Park	
Height (m)	Scale (λ)	Shape (k)	Scale (λ)	Shape (k)
20	3.59	1.36	4.07	1.62
30	4.97	1.97	4.36	1.66
40	5.81	2.27	4.78	1.90
50	6.11	2.39	5.23	2.02

Table 4.2: Weibull curve fit statistics.

the Weibull curve fit fails to capture the peaks and sloping edges of the real distribution. If used in further analysis, for example to estimate the annual energy production of a turbine, the Weibull curve fit would produce inaccurate results.

At the 20m and 30m heights at RIM Park, the number of data points in the lowest bin seems somewhat too high. This could be attributed to data collected under icing conditions, which the filtering process did not eliminate. Rather than removing extra data, the issue should be kept in mind during further analyses.

The shape factors are around 2, which matches with expectations. Higher shape factor indicates stronger winds. Just like the mean wind speeds, the shape factors increase with height, are more sensitive to height at WRESTRC than RIM Park, and are greater at WRESTRC than RIM Park, except at 20m. Based on the mean wind speeds and wind speed distributions, WRESTRC is a more viable site than RIM Park for wind power.

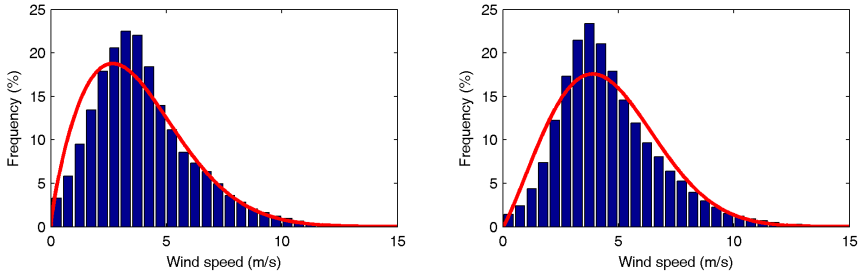

(a) 20m (b) 30m

(c) 40m (d) 50m

Figure 4.1: Wind speed histogram and Weibull fit at WRESTRC.

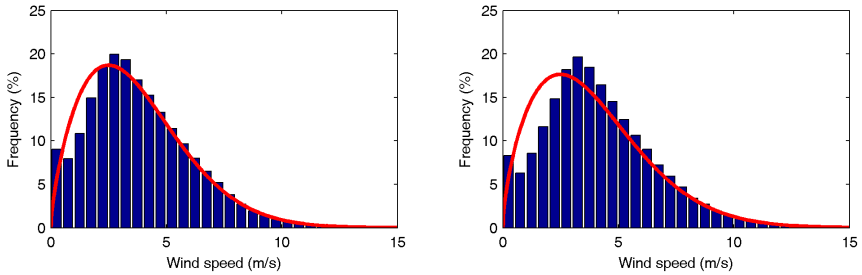

(a) 20m (b) 30m

(c) 40m (d) 50m

Figure 4.2: Wind speed histogram of Weibull fit at RIM Park.

4.3 Wind speed variability

The mean wind speeds vary depending on the time of year and time of day. In this geographical area, wind tends to be stronger in the winter and in the afternoon, as expected. These trends at WRESTRC are shown in Figure 4.3.

The seasonal variation is quite significant; the difference between winter and summer at 50m at WRESTRC in 2009 was roughly 2 m/s, on an annual average of 5.4 m/s. The difference changes from year-to-year so this may be a more extreme case, but the importance is that wind energy production will be noticeably lower during the summer.

The diurnal variation is less pronounced than the seasonal variation. The diurnal variation is largely driven by surface warming, therefore it is more important to consider at low elevations, but the effect diminishes at higher elevations.

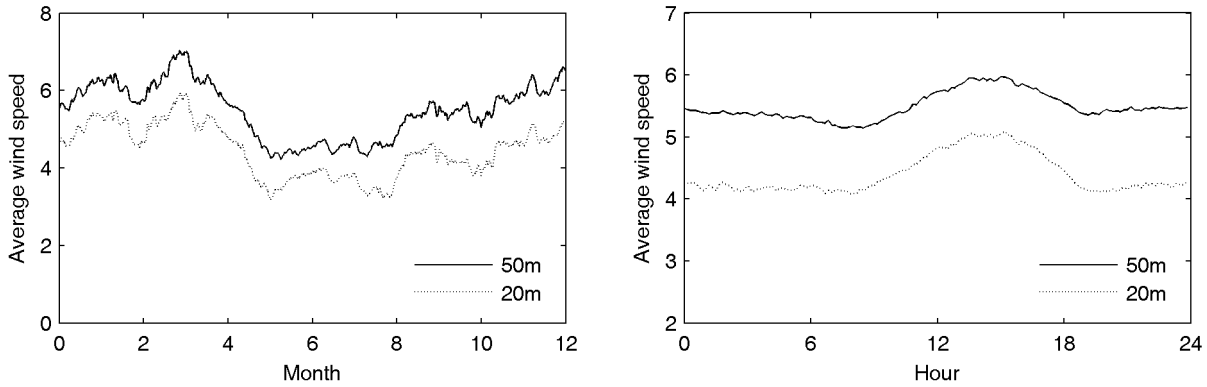

(a) Wind speeds smoothed by 30-day moving average

(b) Wind speeds averaged by time of day

Figure 4.3: Seasonal and diurnal variation at WRESTRC in 2009

4.4 Wind direction

The relationship between wind speed and wind direction was plotted as 2D histograms in polar coordinates in Figure 4.4. Wind direction data is gathered at 30m from the NRG wind vanes, and at 50m from the RMY anemometers.

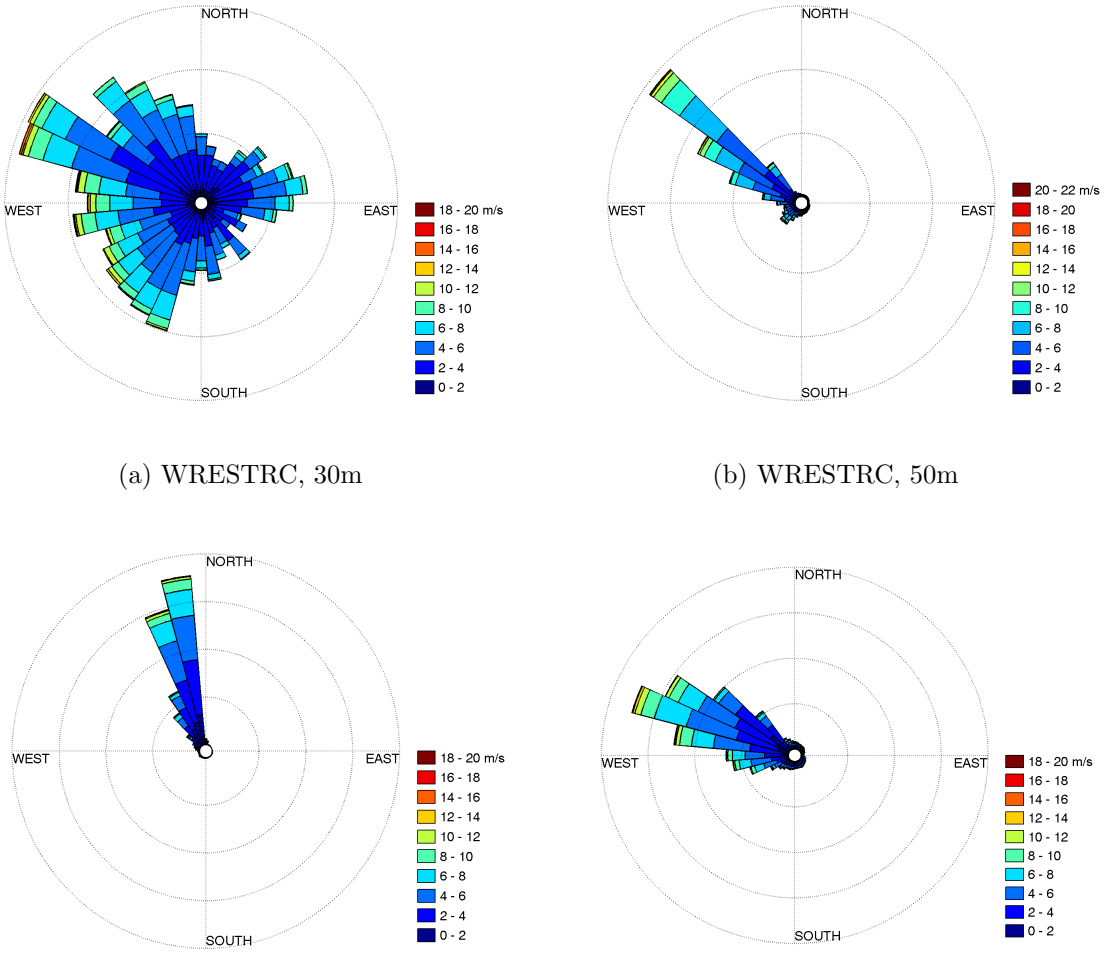

(a) WRESTRC, 30m

(b) WRESTRC, 50m

(c) RIM Park, 30m

(d) RIM Park, 50m

Figure 4.4: Wind rose plots

At WRESTRC, there is a clear dominant wind direction at 50m, but at 30m the wind direction is very inconsistent. This is possibly due to a malfunctioning sensor, but also possibly due to the buildings and trees nearby affecting the flow at 30m, but not at 50m. Unstable, fluctuating wind direction is highly detrimental to wind turbine performance and lifespan. In yawed flow, wind turbines generate less power [57] and undergo dynamic structural loads [58]. If this is the case, a wind turbine should be placed well above 30m to avoid unfavourable flow conditions.

At RIM Park, there is a clear dominant wind direction: from the northwest. There is a roughly 60°offset between the measurements at 30m and 50m, but this is almost certainly

due to the installation process. The aim was to set the wind vanes so that 0°corresponds to due north, but this was not easy since the booms and instruments were fixed to the tower before it was raised. There is nothing in the RIM Park terrain that would cause a wind direction shift at different heights. The actual angle of the dominant wind direction is unimportant, only that the wind direction is consistent.

4.5 Wind shear profile

The mean wind speeds over the 2 year measurement period were plotted against height to give a general idea of the wind shear at each site. The power law and log law profiles, outlined in Section 2.4, were fitted to the site mean wind speeds and graphed in Figure 4.5. The regressions were calculated computationally by minimizing the sum of the square of the errors. The resulting roughness exponents and roughness lengths are listed in Table 4.3.

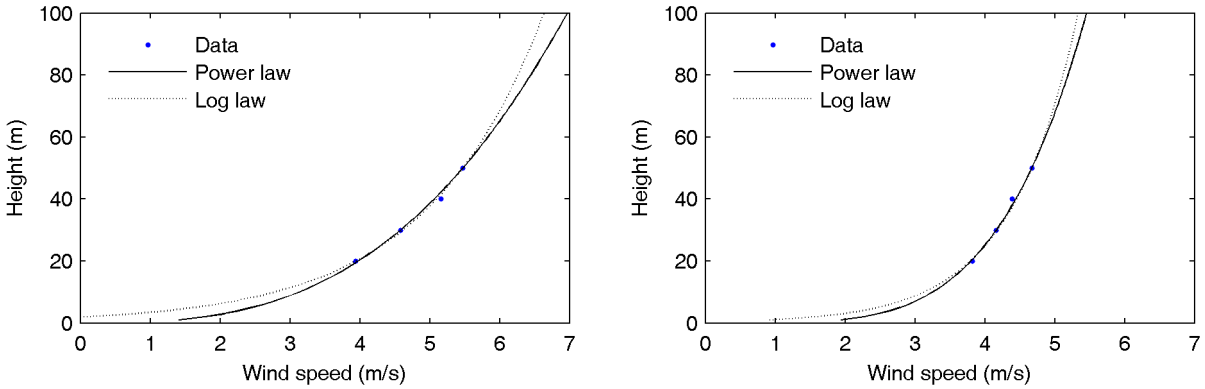

(a) WRESTRC (b) RIM Park

Figure 4.5: Wind shear curves using site mean wind speeds.

	WRESTRC	RIM Park
Roughness exponent (α)	0.34	0.22
Roughness length (m) (z_0)	1.74	0.38

Table 4.3: Wind speed statistics.

Both the power law and log law fit the data well; however, the curves can diverge greatly beyond the measurement range. Extrapolating wind speeds to higher heights may

be necessary for a project, but is difficult to do accurately. Wind shear is typically one of the largest sources of uncertainty in a wind resource assessment [59]. For this project, class IV wind turbines were deemed most appropriate at both sites, which are typically under 50m at hub height. Therefore, wind speed extrapolation was not necessary for further analysis.

WRESTRC has greater wind speeds than RIM Park, but also greater wind shear. Compared to the roughness quantities listed in tables 2.1 and 2.2, WRESTRC roughly corresponds to an urban area and RIM Park corresponds to a forested area. This is not quite accurate, but fairly close. The WRESTRC tower is closely surrounded by trees and small buildings, while the RIM Park tower is in a more open area with some trees.

Wind shear is affected by a number of factors and fluctuates considerably, so describing a site with a single roughness quantity does not give the full picture. The roughness exponent was calculated using every set of wind speed data recorded in 10-minute intervals, and the distributions are plotted in Figure 4.6. Data sets were ignored when data was unavailable at one or more heights.

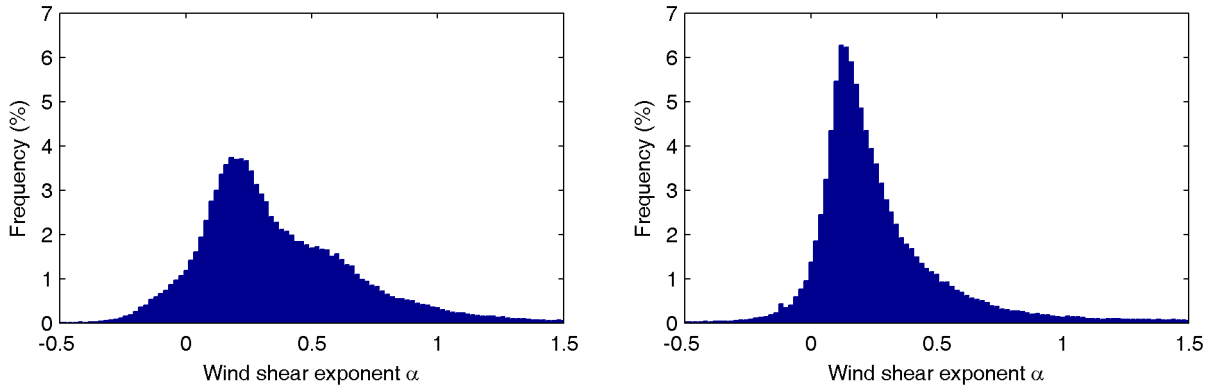

(a) WRESTRC (b) RIM Park

Figure 4.6: Distribution of roughness exponent (α) calculated in 10-minute intervals.

The spread of roughness exponents is much greater at WRESTRC than at RIM Park, likely due to more complex terrain. At both sites, there are times when the roughness exponent is unusually high or low. In a stable boundary layer, the expected wind speed profile has increasing wind speed with increasing height at a decreasing rate, thus the exponent is inside the range of 0 to 1. In an unstable separated boundary layer, there are sections that would correspond to an exponent less than 0 (decreasing wind speed with increasing height) or greater than 1 (increasing wind speed with increasing height at increasing rate). These situations can occur when the flow encounters an adverse pressure gradient [23]. Figure 4.7 is an illustration of these boundary layer situations.

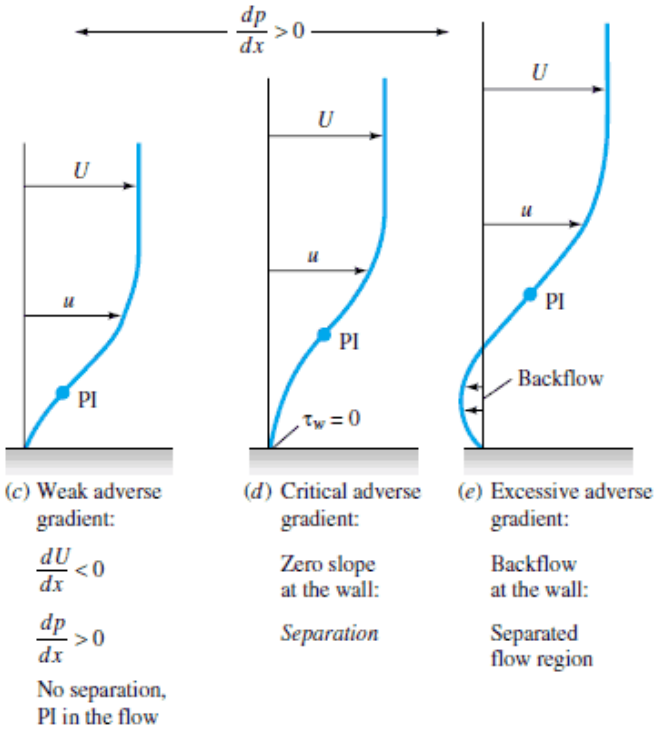

Figure 4.7: Effect of pressure gradient on boundary layer profiles [23]

Roughness exponents outside the expected range tend to occur most often at low wind speeds, but can still occur at high wind speeds. Figure 4.8 contains boxplots showing the distribution of roughness exponents grouped into 1 m/s wind speed bins. The boxes indicate the first quartile, median, and third quartile statistics. The median and interquartile range of roughness exponents both decrease with increasing wind speed. There are fewer data points at higher wind speeds which may explain the smaller range, but it seems natural to believe wind shear is lower and more consistent in strong winds.

Figure 4.9 contains boxplots showing the distribution of roughness exponents grouped into 20°wind direction bins. The effect of wind direction on wind shear is very evident at WRESTRC due to the terrain. When the wind blows from the dominant wind direction, it flows along a flat strip of grass and the roughness exponents are considerably lower. When the wind blows from a non-dominant direction, it flows over trees or buildings, causing higher wind shear. The effect of wind direction on wind shear is weaker at RIM Park, and accordingly, the terrain at RIM Park is similar in all directions. The boxplot does have a slight dip in the dominant wind direction, which is the direction from where the wind blows the strongest. See Figure 3.2 for an overview of the sites.

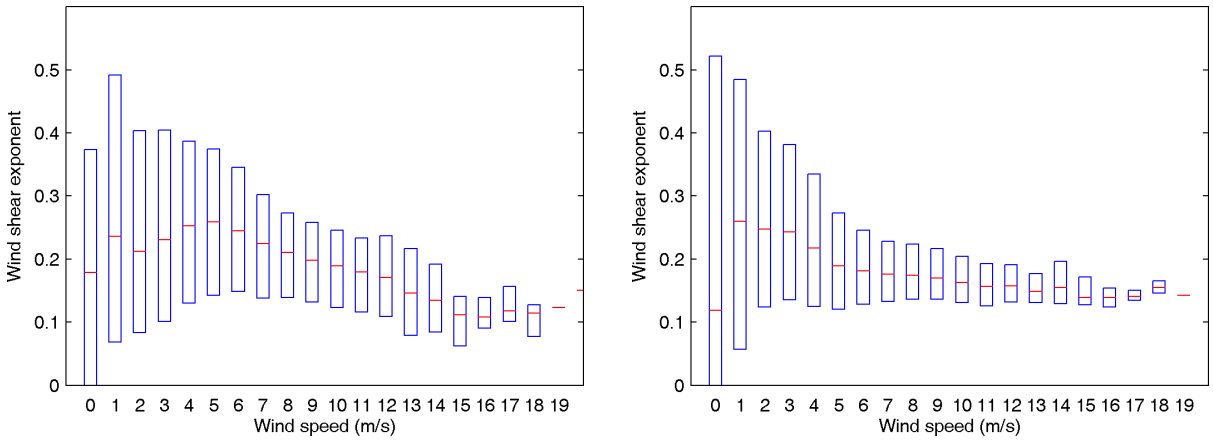

(a) WRESTRC (b) RIM Park

Figure 4.8: Boxplot of roughness exponents in 1 m/s wind speed bins.

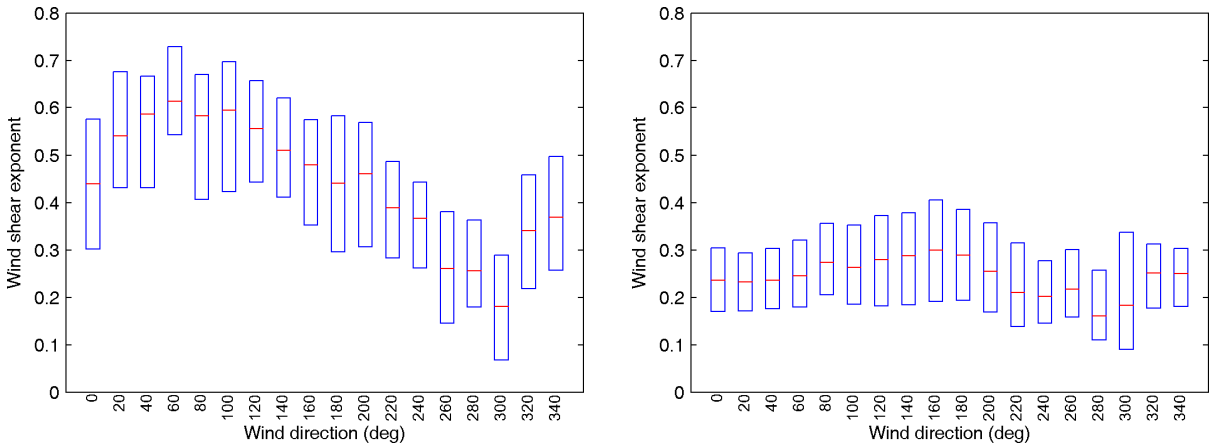

(a) WRESTRC (b) RIM Park

Figure 4.9: Boxplot of roughness exponents in wind direction bins.

4.6 Wind shear power law model

For the above analysis, a simple one-parameter power law model was used to fit the data. The results were adequate overall, but there were times when the one-parameter model did not fit the data satisfactorily. Greater flexibility may help in these cases.

The one-parameter and two-parameter models were fitted for wind speed data sets recorded in 10-minute intervals, using the methods described in Section 2.5. When the

wind speed at one or more heights was unavailable, the entire data set was omitted. Out of the 105120 sets recorded over two years, 71485 sets were analyzed at WRESTRC and 83653 sets were analyzed at RIM Park.

The distributions of root mean square error (RMSE) from the regressions are plotted in Figure 4.10. Overall, the 2-parameter model resulted in lower errors than the 1-parameter model, as expected, but the difference was not significant. As an aside, high RMSEs (greater than 0.5 m/s) occured more often at WRESTRC than at RIM Park. This is likely because situations when the power law model does not fit the velocity profile well occurred more often at WRESTRC.

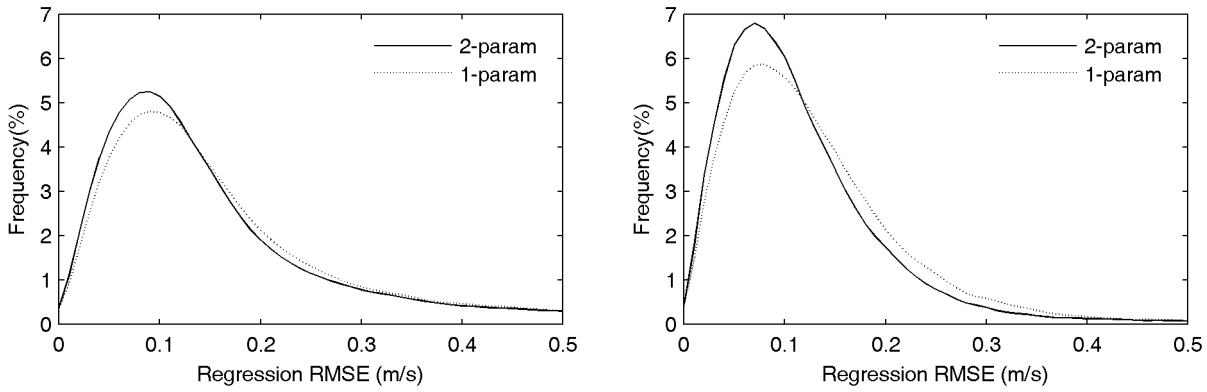

(a) WRESTRC (b) RIM Park

Figure 4.10: Distributions of regression RMSE from one-parameter and two-parameter models.

Reducing the RMSE of the regression will also reduce the uncertainties in the estimated parameters and in the predicted values. This is important given that wind speed extrapolation is a large source of uncertainty in a wind resource assessment. However, it would be better to compare the wind shear models in terms of how accurate the model predictions are.

The 1-parameter and 2-parameter models were fitted to data at 20m, 30m, and 40m, and then used to predict the wind speed at 50m for each 10-minute interval. For the one-parameter model, the wind speed at 40m was used as the reference. Distributions of the differences between predicted wind speeds and actual wind speeds at 50m are shown in Figure 4.11.

Both models have positive skew at WRESTRC, and negative skew at RIM Park. Therefore, it cannot be said that power law models are generally biased one way or the other; it is site-dependent. Looking back to the shapes of the wind speed profiles in Figure 4.5, WRESTRC has a rounder profile while RIM Park has a steeper profile, which may explain

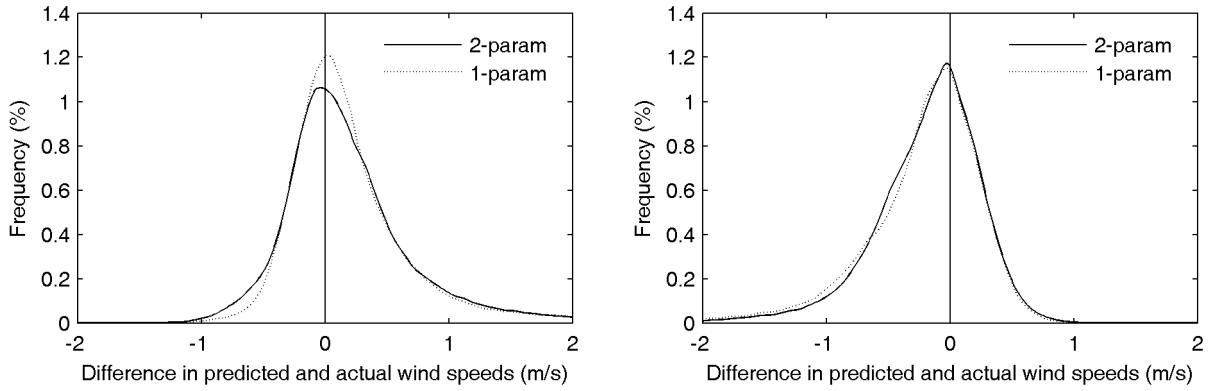

(a) WRESTRC (b) RIM Park

Figure 4.11: Differences between predicted and actual wind speeds from one-parameter and two-parameter models.

why overestimates tend to happen at WRESTRC while underestimates tend to happen at RIM Park.

In the graphs, it is nearly imperceptible whether the 1-parameter or 2-parameter model performs better. The root-mean-squares of the differences were calculated as a measure for comparison, and are listed in Table 4.4.

	WRESTRC	RIM Park
1-param model	0.59 m/s	0.52 m/s
2-param model	0.60 m/s	0.46 m/s

Table 4.4: RMS of the differences between predicted and actual wind speeds

At RIM Park, the 2-parameter model outperforms the 1-parameter model, and the difference is fairly clear. At WRESTRC, the 1-parameter model actually slightly outperforms the 2-parameter, despite being simpler and less flexible. A possible explanation for this is that forcing the curve through the data at 40m can be a benefit, rather than a detriment, when the goal is to extrapolate to 50m. By comparison, if the 1-parameter model is forced through 20m instead, the RMS of the differences between predicted and actual wind speeds at 50m would be 0.62 m/s, which is much worse than the 2-parameter model. Another thing to note is that the flow at WRESTRC is more complex than at RIM Park, and times when the power law profile is not a good fit may be distorting the results.

In terms of goodness-of-fit, the 2-parameter power law wind shear model does perform

better than the 1-parameter model, as expected, and the added computational complexity was not overbearing. In terms of accuracy of extrapolation, the 1-parameter may have an advantage of fitting perfectly through the reference height, whereas the 2-parameter fits closer to all the data points in total. But the difference seen at WRESTRC was almost insignificant, so the 2-parameter model should be recommended at any site. A weighted, 2-parameter regression may be an even better solution.

4.7 Turbulence intensity

Turbulence intensity was calculated as the standard deviation over the mean wind speed for each 10 minute interval as shown in Equation 2.16. Scatter plots of turbulence intensity versus mean wind speed are in Figures 4.12 and 4.13, along with the IEC design specifications. Comparing the scatter of data to the design curves, at lower heights, a class A wind turbine designed for high turbulence is needed. Even at 50m, a class A wind turbine would be appropriate. An outline of the wind turbine classes was provided in Section 2.7.

Turbulence intensity is affected by numerous factors, including height, wind speed, and wind direction. Table 4.5 of mean turbulence intensities shows that turbulence intensity decreases with increasing height. This relationship is stronger at WRESTRC than at RIM Park. Furthermore, turbulence intensity is generally lower at WRESTRC than at RIM Park, except at 20m, where the turbulence is notably higher. This could be due to the trees and buildings near the WRESTRC tower affecting flow at low heights.

Height (m)	WRESTRC	RIM Park
20	0.245	0.220
30	0.205	0.207
40	0.176	0.187
50	0.160	0.177

Table 4.5: Mean turbulence intensity at varying heights

The graphs of turbulence intensity versus mean wind speed in Figures 4.12 and 4.13 are somewhat misleading. Since the denominator of turbulence intensity is the mean wind speed, the scatter is influenced by a $1/x$ trend. There appears to be high variability at low wind speeds, and then the scatter converges at high wind speeds.

The scatter plots in Figures 4.14 and 4.15 are of standard deviation versus mean wind speed. The turbulence intensity decreases with mean wind speed, but the standard devia-

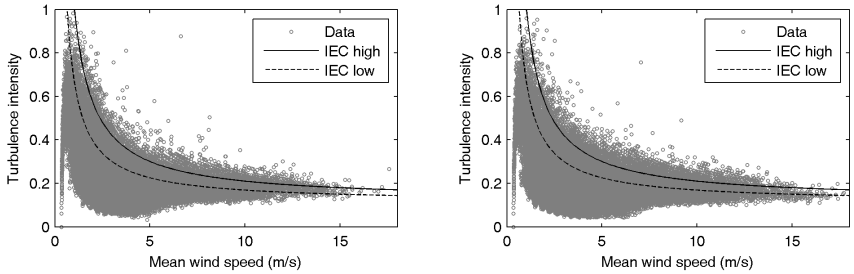

(a) 20m (b) 30m

(c) 40m (d) 50m

Figure 4.12: Turbulence intensity at WRESTRC.

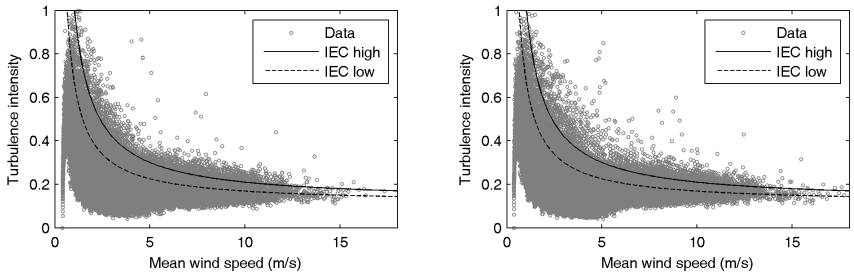

(a) 20m (b) 30m

(c) 40m (d) 50m

Figure 4.13: Turbulence intensity at RIM Park.

tion increases with mean wind speed, though at a slower rate than 1:1. The variability of the scatter is roughly even and does not actually converge at high mean wind speed.

Linear regressions were added to the plots. The lines suggest that the standard deviation of wind speed decreases very slightly with increasing height, but the relationship is very weak.

Table 4.6 summarizes how turbulence intensity is affected by height and mean wind speed, and the inter-relationships involved.

	Increasing height	Increasing mean wind speed
Std dev wind speed	small decrease	increase, slower than 1
Mean wind speed	increase	1
Turbulence intensity	decrease	decrease

Table 4.6: Effect of height and mean wind speed on turbulence intensity

The distribution of turbulence intensity grouped into 20°wind direction bins is illustrated in the boxplots in Figures 4.16 and 4.17. The turbulence intensity dips lower in the dominant wind direction, but overall, the relationship between turbulence and wind direction is fairly weak. The exception is at 20m at WRESTRC, where turbulence intensity exhibits a similar relationship as the one between wind shear and wind direction (see Fig 4.9). The reason for this is again, the terrain. When the wind blows from the dominant wind direction, it flows along a flat strip of grass, and turbulence is low. When the wind blows from a non-dominant direction, it flows over trees or buildings, causing higher turbulence. However, the effect of the trees, which are less than 10m tall, is weak at 30m and negligible at 40m. A wind turbine should be placed above 30m to avoid the high turbulence intensity caused by the terrain.

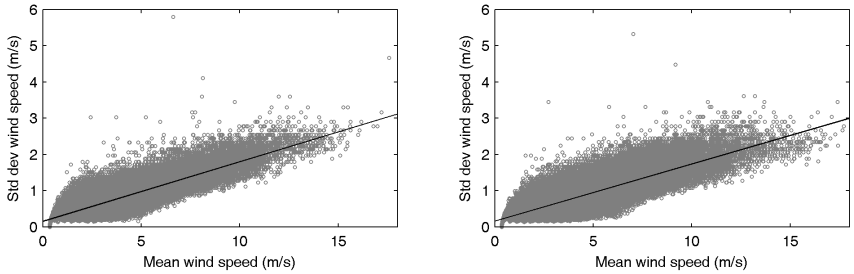

(a) 20m

(b) 30m

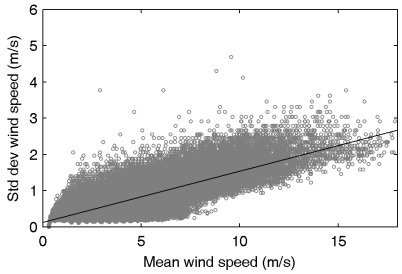

(c) 40m

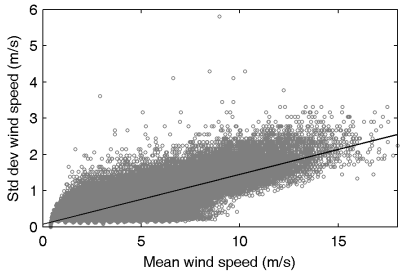

(d) 50m

Figure 4.14: Standard deviation vs. mean wind speed at WRESTRC.

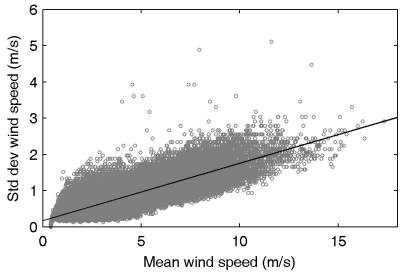

(a) 20m

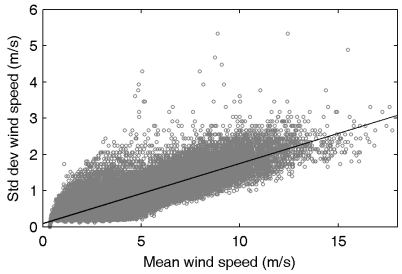

(b) 30m

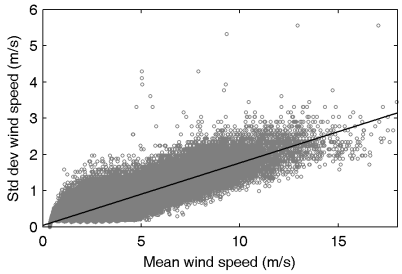

(c) 40m

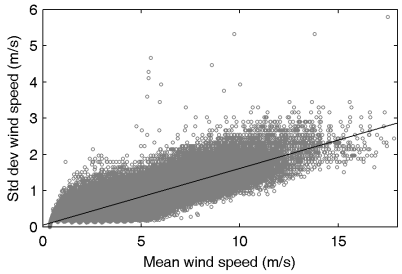

(d) 50m

Figure 4.15: Standard deviation vs. mean wind speed at RIM Park.

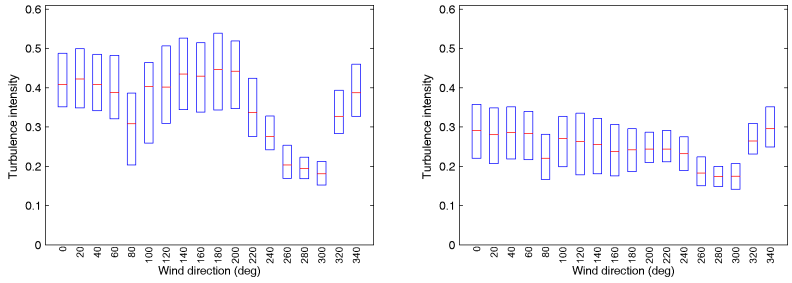

(a) 20m (b) 30m

(c) 40m (d) 50m

Figure 4.16: Boxplots of turbulence intensity in wind direction bins at WRESTRC.

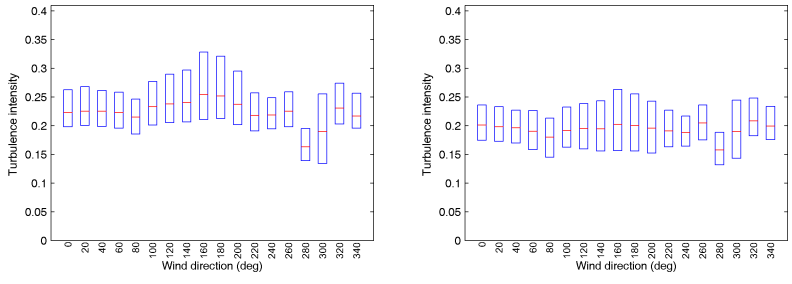

(a) 20m (b) 30m

(c) 40m (d) 50m

Figure 4.17: Boxplots of turbulence intensity in wind direction bins at RIM Park.

4.8 Turbulence intensity and time interval

The turbulence intensities calculated in the above section were for 10 minute time intervals, during which 300 samples are taken. In a steady flow, the time interval should not matter as long as enough samples are taken. Of course, the flow of air near the surface of the earth is unsteady, so the data recording interval may have an effect on the perceived turbulence intensity. The IEC specifications indicate that data should be sampled at 1 Hz and recorded every 10 minutes [28], but not all met towers and weather stations do so. One minute and one hour are the other common choices.

The turbulence intensity was re-calculated to cover longer time intervals. The raw data was unavailable, but fortunately the number of samples in each data set was known and constant. Using the mean wind speed and standard deviation from each individual data set (U_i and σ_i), the longer-term mean wind speed and standard deviation that covers from the first to the ith data sets ($U_{1,i}$ and $\sigma_{1,i}$) can be calculated using these equations. They are derived from the definitions of mean and standard deviation.

$$U_{1,i} = \frac{(i-1)U_{1,i-1} + (1)U_i}{i} \tag{4.1}$$

$$\sigma_{1,i} = \frac{(i-1)[\sigma_{1,i-1} + (U_{1,i-1} - U_{1,i})^2] + (1)[\sigma_i + (U_i - U_{1,i})^2]}{i} \tag{4.2}$$

Table 4.7 lists the mean turbulence intensities at 50m that would be perceived if the recording interval was longer.

Time interval	WRESTRC	RIM Park
10 minute	0.160	0.177
1 hour	0.195	0.224
24 hours	0.329	0.400

Table 4.7: Mean turbulence intensities at 50m with different recording intervals

Perceived turbulence intensity increases significantly with time interval; it is as influential a factor as height from the ground. The IEC specifications are intended for a 10 minute sampling rate, therefore the site data should match this before comparing the scatter of turbulence intensity to the design curves. Faster-sampled data can be recalculated to 10 minutes, but nothing can be done with slower-sampled data. Furthermore, when

comparing turbulence intensity from different data sources, the time interval needs to be equal, otherwise the results would be misleading.

To look at even longer time intervals, the relationship between mean turbulence intensity and number of data sets is plotted on log-log axes in Figure 4.18. Note that there are 144 sets in 1 day, 1008 sets in 1 week, and 52560 sets in 1 year.

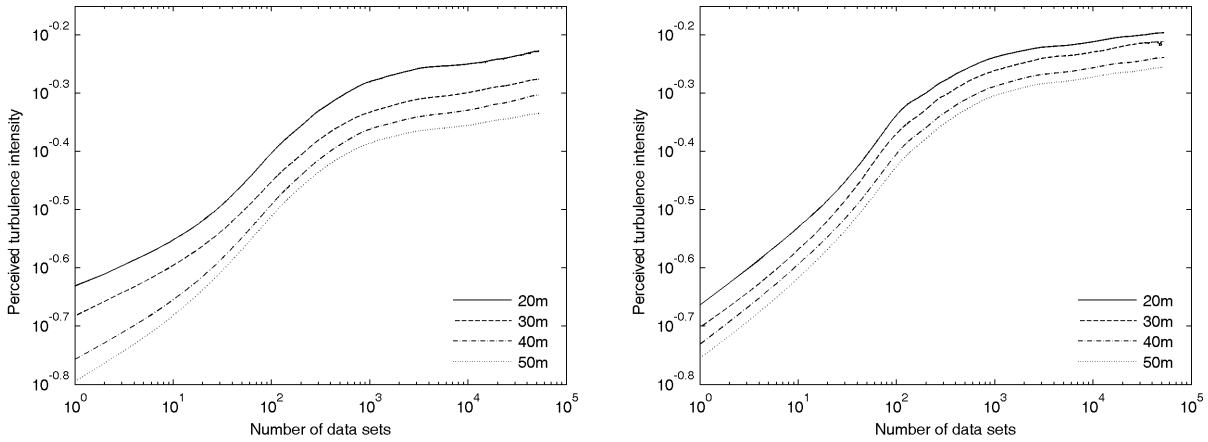

(a) WRESTRC (b) RIM Park

Figure 4.18: Perceived turbulence intensity over longer time periods.

There is a consistent shape in all the curves. Turbulence intensity increases with time interval, but after 1 week, the increase is much slower. The curves do not appear to plateau, but continue to increase steadily past the 1 year mark. The turbulence intensity over such long time intervals is likely a not useful value to know, but one benefit of these plots is that some trends are easy to observe:

1. Turbulence intensity decreases with increasing height
2. Turbulence intensity is more sensitive to height at WRESTRC than at RIM Park
3. Turbulence intensity is lower at WRESTRC than RIM Park

Unlike the scatter plots in the previous section, the plots of turbulence intensity versus time interval immediately convey these relationships and comparisons. However, the computational time required to generate these plots was prohibitively expensive. Therefore, calculating long-term turbulence to such an extent is not practical for a wind resource assessment. The trends can be gleaned from the summary statistics.

4.9 Wind turbine power curve model

For simplicity, a linear 1 kW power curve, given by Equation 4.3, was assumed in the estimations of annual energy production (AEP). The attributes of a power curve were discussed in Section 2.8. The AEP results obtained with this simplified model will give a rough impression of the wind energy potential at each site. Furthermore, the results can be scaled up. For example, a 10 kW capacity turbine would produce 10 times the energy, assuming the cut-in, rated, and cut-out wind speeds are the same.

$$P(U) = \begin{cases} 0 & U < U_{cut-in} \\ P_{rated}\left(\dfrac{U - U_{cut-in}}{U_{rated} - U_{cut-in}}\right) & U_{cut-in} \leq U < U_{rated} \\ P_{rated} & U_{rated} \leq U < U_{cut-out} \\ 0 & U \geq U_{cut-out} \end{cases} \tag{4.3}$$

To get an idea of appropriate values for the cut-in, rated, and cut-out wind speeds, specifications were found for several small wind turbines and listed in Table 4.8 [60, 61, 62, 63, 64, 65]. These turbines are available from various dealers in Canada.

Model	Rated power (kW)	Cut-in WS (m/s)	Rated WS (m/s)	Cut-out WS (m/s)
Skystream 3.7 [60]	2.1	3	11	–
Endurance S-343 [61]	5.2	4.1	11	24
Sonkyo Windspot [62]	7.5	3	12	–
Bergey Excel 10 [63]	10	3.4	12	–
Wind Solutions 50 [64]	50	3	10	25
Seaforth AOC 15/50 [65]	50	4.9	11.3	22.4

Table 4.8: Power curve specifications of small wind turbines.

The cut-in, rated, and cut-out wind speeds were set to 4 m/s, 12 m/s, and 25 m/s respectively. The finalized power curve model is pictured in Figure 4.19.

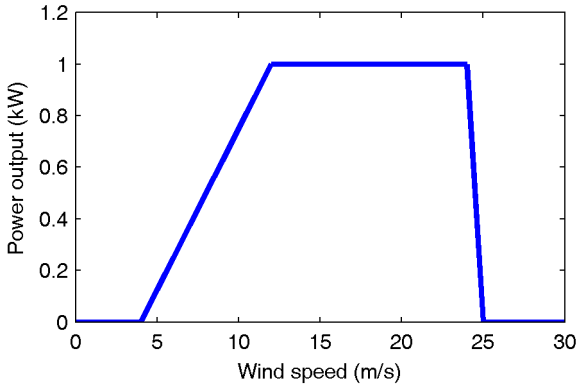

Figure 4.19: Theoretical 1 kW power curve used for AEP estimates.

4.10 Annual energy production

Two methods were used to calculate the expected annual energy production (AEP) from the meteorological data collected in 2009 and 2010 inclusive. The time series method involves using every wind speed data point, and integrating power over time. The histogram method involves the histogram of wind speed, and integrating over the bins. There is some loss of data when using the histogram method, but it is common practice in industry with a 1 m/s bin size. The wind speed histogram has other applications in a wind resource assessment, so the time series method is considered more computationally intensive.

Results from the time series method are in Table 4.9 in units of gigajoules and megawatt-hours. As expected, AEP increases with height and is higher at WRESTRC than RIM Park. These are the same trends as with mean wind speed, but more dramatic. For example, the mean wind speed at WRESTRC is 4.0 m/s at 20 m and 5.5 m/s at 50 m, while the AEP more than doubles between 20 m and 50 m.

	WRESTRC		RIM Park	
Height (m)	GJ	MWh	GJ	MWh
20	2.96	0.82	3.09	0.86
30	4.29	1.19	3.62	1.01
40	6.05	1.68	4.22	1.17
50	6.91	1.92	4.88	1.36

Table 4.9: Annual energy production estimates using time-series data

With this data, a proposed wind turbine can be sized for a given load. According to a 2007 Households and Environment study by Statistics Canada, an annual average of 40 GJ (or 11 MWh) of electricity is consumed per household [66]. Therefore, 5 kW to 15 kW wind turbines would be generally appropriate to offset the consumption of a household.

The histogram method was tested using five different bin sizes: 0.1 m/s, 0.3 m/s, 0.5 m/s, 0.8 m/s, and 1 m/s. The ratios of the AEP results from the histogram method over the time series method are graphed in Figure 4.20.

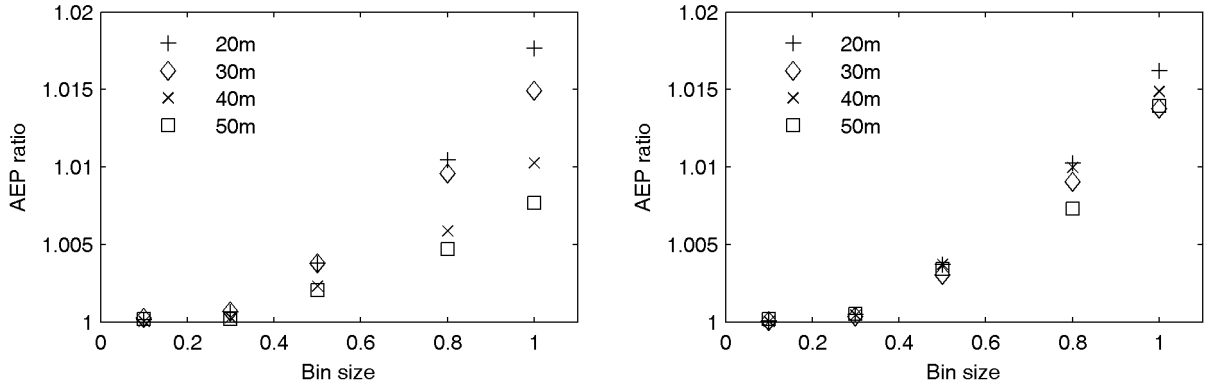

(a) WRESTRC (b) RIM Park

Figure 4.20: Ratio of AEP from the histogram method and the time series method.

In all cases, the histogram method yielded higher AEP estimates than the time series method, but even with 1 m/s bins, the differences were less than 2%. This may be an acceptable level of error depending on the project. Still, it should be noted that decreasing bin size can reduce the differences significantly. With 0.5 m/s bins, the histogram estimates are less than 0.5% over; and with 0.1 m/s bins, less than 0.03% over.

The reason the histogram method overestimates the AEP at these sites is likely because of the shape of the wind speed distribution, and because the bin centres were used to represent each bin. Depending on the slope and concavity of a segment of a distribution, the rectangular area of the bin (based on the centre) may be an overestimate or underestimate of the actual area under the segment. With the power curve factored in, which gives more weight to higher wind speed bins, the segments of the wind speed distribution resulting in overestimate simply outweigh the segments resulting in underestimate. It's plausible that at other sites, the histogram method could underestimate the AEP, depending on the wind speed distribution and power curve.

4.11 Capacity factor

The capacity factors were calculated as the AEP divided by the total energy production potential, as given in Equation 2.24. The results are listed in Table 4.10.

Height (m)	WRESTRC	RIM Park
20	9.38	9.80
30	13.6	11.5
40	19.2	14.2
50	21.9	15.5

Table 4.10: Capacity factors

The results indicate that neither site would be appropriate for a commercial wind farm. A wind turbine at WRESTRC with a hub height above 50m might approach feasibility, depending on the financial situation and if the wind turbine is designed for lower wind speeds.

4.12 Measure-Correlate-Predict

Long-term wind speed and wind direction data were gathered from three weather stations – WRESTRC, the University, and the airport – for a Measure-Correlate-Predict (MCP) analysis, as previously described in Section 2.11. With data spanning multiple years, a better picture of the sites' lifetime wind characteristics could be garnered. The mean wind speeds over time, smoothed by a sixteen-week moving average, at the WRESTRC met tower (50m only) and the weather stations are plotted in Figure 4.21.

At this time scale, there is visible correlation in wind speeds among the sites; they follow the same trend and generally increase and decrease together. The year-to-year variation is only slightly visible, as the seasonal variation is much more pronounced.

The years 2004 to 2009 inclusive are available at all weather stations, so this subset of data was used for the purpose of an even comparison. The variability in annual mean wind speeds over these years was 3.0% at WRESTRC, 3.5% at the airport, and 4.0% at the University. A figure of 6% is typically assumed as the lifetime inter-annual variability at any site [43], and values of 3-4% over six years seems roughly in line.

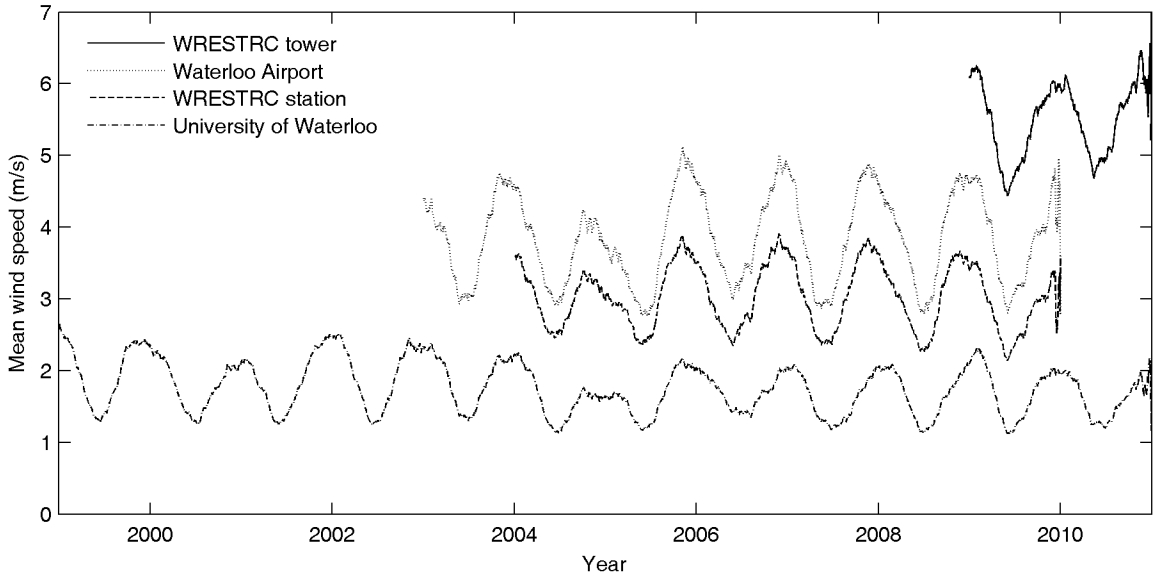

Figure 4.21: Mean wind speeds over time at the WRESTRC met tower and weather stations.

In Figure 4.21, it can be seen that the wind speeds at the University weather station are unusually low. This is largely due to the terrain and the fact that the anemometer is mounted only 3m from the ground; the standard is 10m [40]. The wind speeds at the other two weather stations are at a reasonable level, while the 50m wind speeds at the met towers are noticeably higher.

Another issue is that the airport weather station reported wind speeds to the nearest 1 km/h, or approximately 0.28 m/s. The low precision is obvious in scatter plots of the raw data.

The wind speed data was re-averaged into 1 hour intervals to match the slowest recording rate. Wind speed data from the met towers was removed when the 50m wind direction was outside the dominant range. These ranges were arbitrarily set to 275°-330°at WRESTRC, and 260°-320°at RIM Park. (The wind rose plots at the met towers were previously shown in Figure 4.4.) This resulted in close to 30% of the data being culled at both sites. The wind rose plots at the weather stations are shown in Figure 4.22, and did not indicate any strong dominant wind direction, hence there was no filtering on this data.

The correlations between met towers and reference weather stations during the year 2009 are plotted in Figure 4.23. Met tower data at 50m was used. Simple linear regressions were applied to each relationship, and the correlation coefficients are included on the plots.

The University weather station had the poorest correlation with the met towers, as well as having unusually low wind speeds. The airport weather station had much stronger

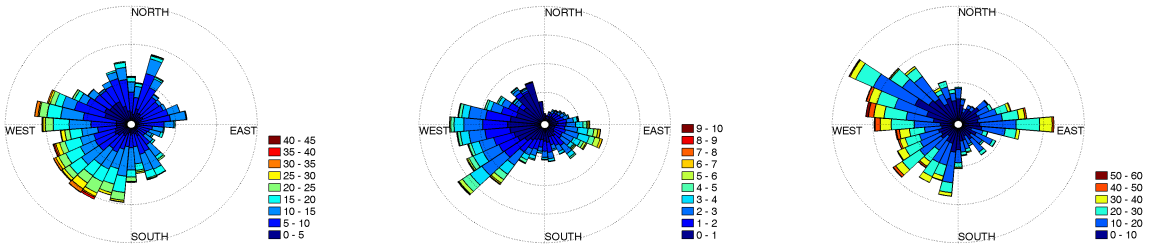

(a) WRESTRC (b) University (c) Airport

Figure 4.22: Wind rose plots at the three weather stations.

correlation, particularly with RIM Park, despite its low precision. However, if the airport wind speeds were used to predict the long-term site wind speeds, the predictions would take visibly discrete values as well.

The WRESTRC weather station had consistently good correlation with both sites, and was considered the best choice of reference for the MCP analysis. The wind speed distribution at this weather station was markedly different from the distributions at the met towers, however, as shown in Figure 4.24. The weather station exhibited lower mean wind speeds and lower variance.

The parameters of the linear regressions between the wind speeds at the WRESTRC weather station and at the 50m met towers are listed in Table 4.11. Both ordinary least squares and variance ratio methods were explored, as explained in Section 2.11.

	WRESTRC		RIM Park	
	OLS	VAR	OLS	VAR
Slope	1.04	1.25	1.10	1.34
Intercept	2.31	1.65	1.47	0.78

Table 4.11: Linear regressions between site and reference wind speeds.

The linear regressions were applied to the five additional years (2004-2008 inclusive) of hourly wind speed data available from the WRESTRC weather station to estimate the wind speeds at the WRESTRC and RIM Park met towers at 50m. The resulting wind speed distributions are plotted in Figure 4.25.

Figure 4.25 illustrates the difference between the two methods. With least squares, the estimated wind speed distributions resemble the reference weather station distribution

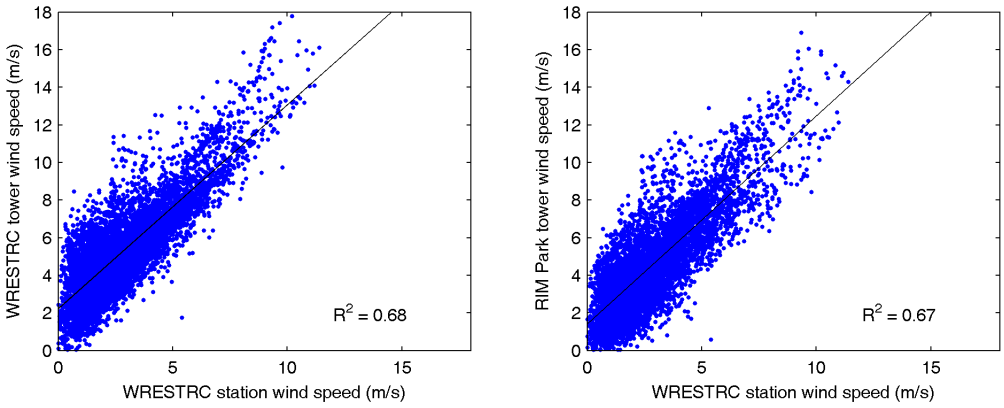

(a) WRESTRC - WRESTRC

(b) RIM Park - WRESTRC

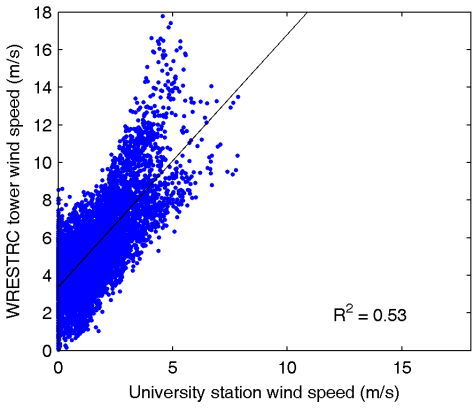

(c) WRESTRC - University

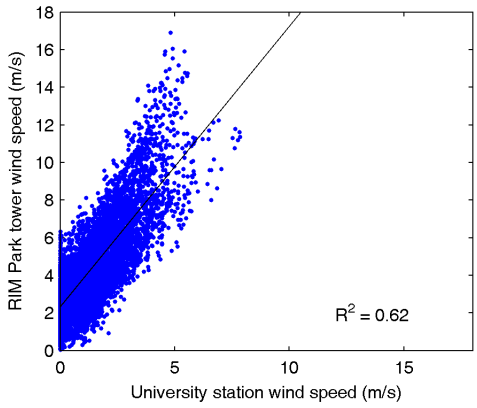

(d) RIM Park - University

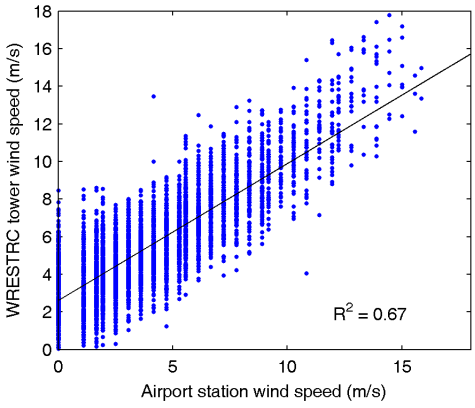

(e) WRESTRC - Airport

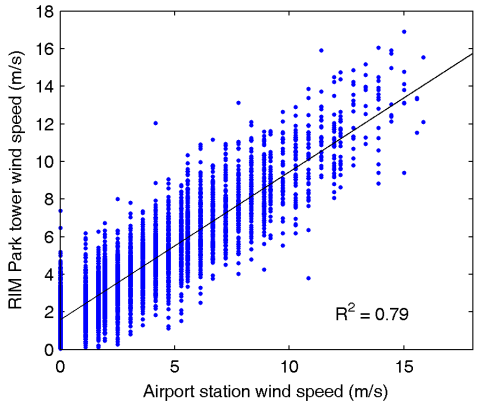

(f) RIM Park - Airport

Figure 4.23: Concurrent wind speed correlations between met towers and weather stations.

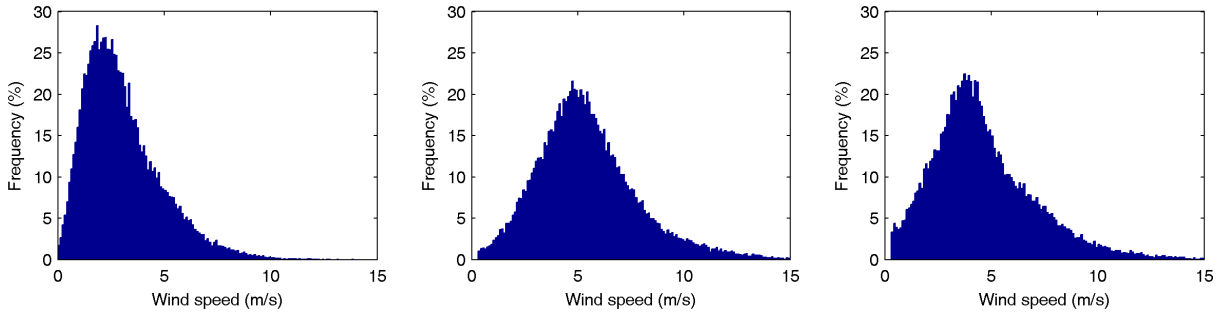

(a) Weather station (b) WRESTRC tower (50m) (c) RIM Park tower (50m)

Figure 4.24: Wind speed distribution at the reference weather station and the met towers.

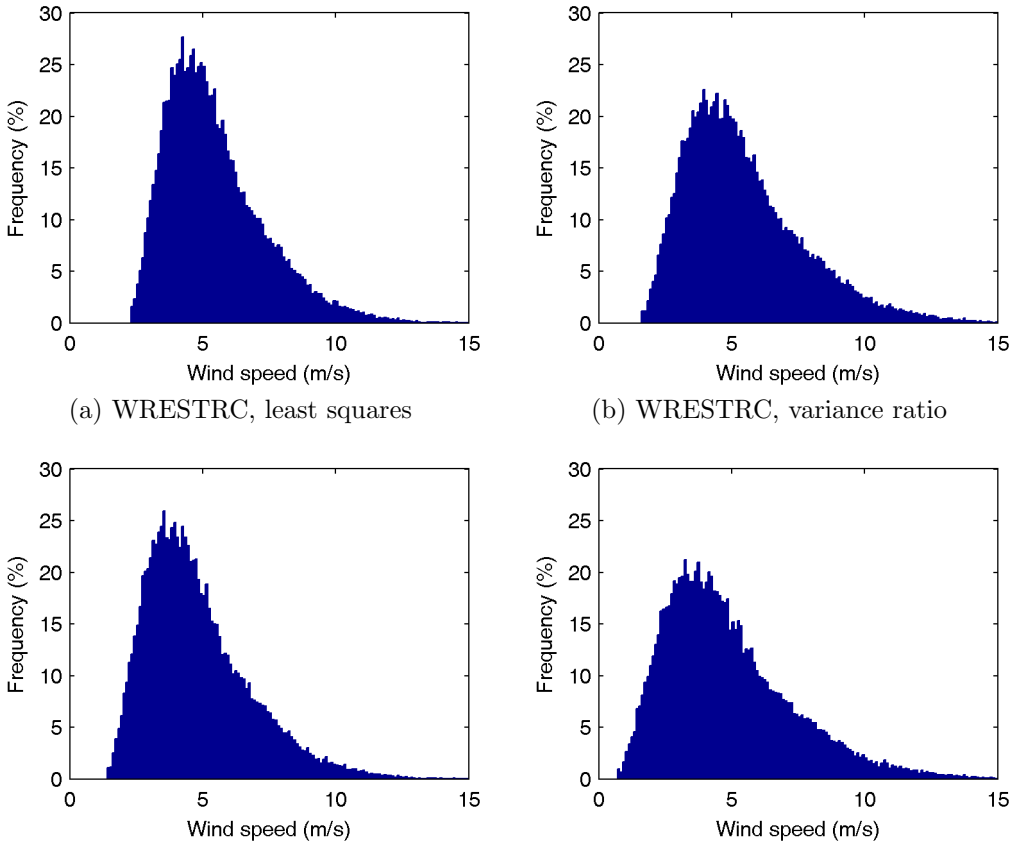

(a) WRESTRC, least squares (b) WRESTRC, variance ratio

(c) RIM Park, least squares (d) RIM Park, variance ratio

Figure 4.25: Estimated long term wind speed distributions.

more; with variance ratio, the estimated distributions resemble the original met tower distributions more. The latter is a more reasonable outcome. This figure also highlights one of the problems with simple linear regressions: the estimated distributions exclude wind speeds below the intercept. Other MCP models address this issue, for example by fitting a parabola through the origin for low wind speeds, and a line for higher wind speeds.

The time series method was used to estimate the AEP from the estimated long-term wind data. The results are tabulated in Table 4.12.

	WRESTRC		RIM Park	
	GJ	MWh	GJ	MWh
Original estimate	6.91	1.92	4.88	1.36
Least squares estimate	6.21	1.72	4.61	1.28
Variance ratio estimate	6.56	1.82	5.28	1.47

Table 4.12: AEP estimates before and after MCP analysis.

The least squares solution resulted in lower AEP than the variance squares solution, which is expected because it estimated wind speed distributions with lower mean and lower variance, similar to the reference weather station distribution.

At WRESTRC, both solutions resulted in lower AEP than the original estimate without MCP analysis. This would suggest that 2009 and 2010 experienced slightly stronger wind speeds than the preceding years. However, at RIM Park, the variance ratio solution resulted in a higher AEP.

Different MCP methods will have different results. Without the actual long-term data measured at the target sites, it is impossible to comment on which MCP method is more accurate.

4.13 Uncertainty analysis

A brief uncertainty analysis can be explored with the meteorological data available. However, a lot of information is unknown that would be required for a complete wind resource assessment in the context of a specific project.

One of the sources of energy loss that can be considered is the air density correction, assuming dry air, since neither met tower was equipped with a humidity sensor. However,

density varies weakly with humidity, particularly at low temperatures. Using the temperature and pressure data recorded in 10-minute intervals over 2009 and 2010, the mean air density was calculated, and the distribution is shown in Figure 4.26.

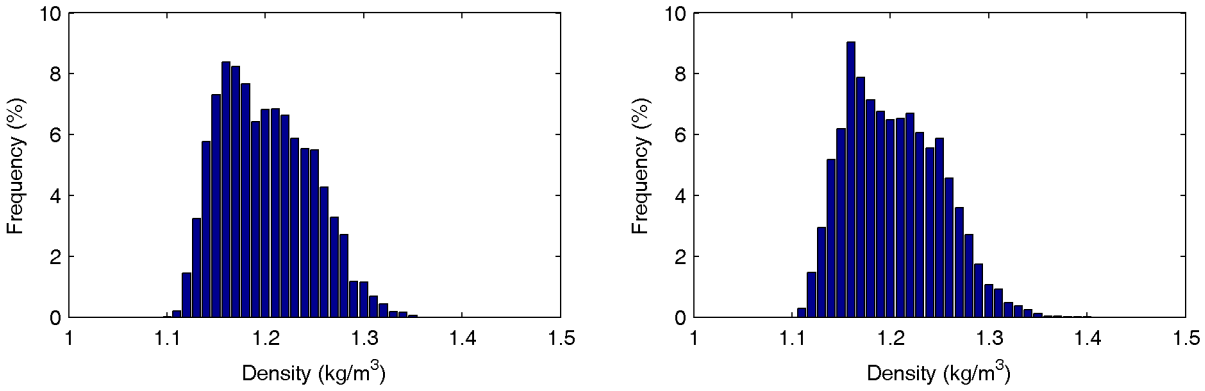

(a) WRESTRC (b) RIM Park

Figure 4.26: Histogram of air density.

The median air density was 1.202 kg/m^3 at WRESTRC and 1.205 kg/m^3 at RIM Park, which are 1.9% and 1.7% lower than the standard 1.225 kg/m^3 assumed for power curve measurement respectively. The power available in the flow is linearly proportional to the density, and the distribution of density is fairly equal above and below the median. Therefore, the AEP estimates at all heights should be lowered by those percentages. The difference is quite minor here, but in other parts of the world, the air density could vary more significantly from the standard.

One of the sources of uncertainty that can be considered is the wind speed measurement uncertainty. This can be attributed to two things (among others): the standard deviation in the 10-minute readings, and the accuracy of the anemometers. Assuming these factors are independent, they can be combined in quadrature. The scatter of standard deviation vs mean wind speed was plotted in Figures 4.14 and 4.15, which provides a sense of those values. The anemometer uncertainty was provided by the manufacturer as Equation 2.34. After seeing the wind characteristics of both sites, the K value for complex terrain and high turbulence was used. This relation is pictured in Figure 4.27.

Strictly speaking, the uncertainty in wind speed can be translated to the uncertainty in the power output by taking the derivative of the power curve and saying $\delta P = (dP/dU)\delta U$. However, above the cut-off wind speed, the power output was assumed to be at a constant level. Taking the derivative would result in zero uncertainty, which is unreasonable. Therefore, the derivative of the linear piece was applied to the entire curve.

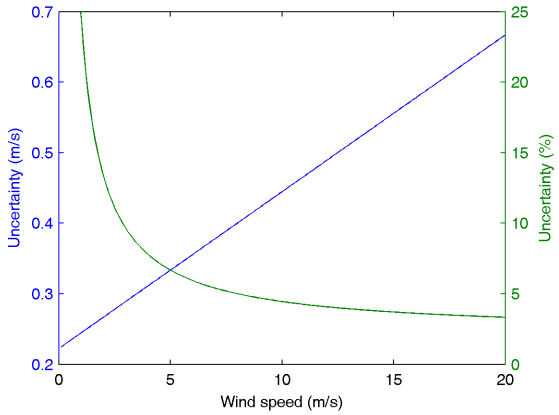

Figure 4.27: NRG #40C anemometer uncertainty.

$$\delta P = \left(\frac{P_{rated}}{U_{rated} - U_{cut-in}} \right) \delta U \tag{4.4}$$

The time series method of calculating AEP involved taking the power output during every 10-minute interval, and summing over time. Accordingly, the uncertainties in power output during every 10-minute interval were summed in quadrature, which is to say, the square root of the sum of the squares.

The resulting uncertainties in AEP specifically due to wind speed measurement uncertainty ranged from 0.02 GJ to 0.03 GJ at the four heights at both sites. In comparison, the values of AEP ranged from 2.96 GJ to 6.91 GJ. Therefore, anemometer uncertainty seems to be a relatively small source of uncertainty. In fact, a presentation by Briggs [59] estimates it typically accounts for 7% of the total AEP uncertainty.

Chapter 5

Conclusion

Wind speed, wind direction, temperature and pressure data was collected for over two years at two sites in the Waterloo region, WRESTRC and RIM Park, using 50m tall meteorological towers. A preliminary feasibility study of the wind power potential was conducted, and certain aspects of wind resource assessments were explored.

Small wind turbines less than 50 kW in capacity would be appropriate at both sites, since the mean wind speeds are relatively low for a wind power project. Although the Weibull probability function did not fit the wind speed distributions at either site well, the Weibull shape parameters were in line with expectations. The mean wind speeds varied with time of year and time of day; they tended to be stronger during the winter and during the afternoon, therefore power output will be higher during these times. Both sites exhibited a strong dominant wind direction, which is beneficial.

Mean wind speed increased with height above ground, as expected. The wind shear parameters of the power law model and log law model matched fairly well to the terrain description, and the effect of the terrain on the roughness exponents was visible. At WRESTRC, when the wind flowed from the dominant wind direction, it flowed along a flat strip of grass and the roughness exponents were relatively moderate. When the wind flowed from a non-dominant direction, it flowed over trees or buildings and the roughness exponents were quite high. At RIM Park, the terrain is fairly consistent and flat in all directions, and consequently the roughness exponents were fairly consistent and moderate as well.

A two-parameter power law model of wind shear was explored and compared with the standard one-parameter model. In terms of goodness-of-fit, the two-parameter model did perform better. But in terms of accuracy of prediction, it was not conclusively better or worse than a one-parameter model forced through the known data point closest to the prediction.

Turbulence intensity decreased with increasing mean wind speed and increasing height, as expected. This is slightly misleading, however. Turbulence intensity is the ratio of the standard deviation over the mean wind speed. The standard deviation actually increased with the mean wind speed, but at a slower rate than 1, therefore the turbulence intensity decreased. Comparing to the IEC trend lines, wind turbines designed for high turbulence intensity are recommended at both sites. At WRESTRC, the turbulence intensity was higher when the wind flowed from non-dominant direction at 30m and especially at 20m, due to the terrain.

The relationship between turbulence intensity and measurement interval was also explored. Since atmospheric flow is unsteady, they are not independent. The perceived turbulence intensity was found to increase exponentially with time intervals under 24 hours.

The annual energy production was calculated using two methods: (1) using every wind speed data point and integrating over time, and (2) using the histogram of wind speed and integrating over the bins. The histogram method was found to estimate higher AEP than the time series method, but even with 1 m/s bins, the difference was less than 2%.

The AEP values suggest a 5 kW to 15 kW wind turbine would be appropriate to offset the electricity consumption of a single household, depending on the hub height, in areas similar to WRESTRC and RIM Park. The capacity factors ranged from 9.4% to 22% depending on the hub height, which is not nearly high enough to suggest a commercial wind farm would be viable at either site.

Two measure-correlate-predict methods were investigated, using long-term data from a weather station at WRESTRC for reference. Both methods resulted in lower AEP estimates, but without long-term data at the met towers, the accuracy of the MCP estimates can't be commented on reliably. However, the estimated long-term wind speed distribution resulting from the variance ratio method resembled each site's short-term wind speed distribution much more than the simple linear regression method. Therefore, the variance ratio method performed as expected.

The wind speed distribution and estimated AEP were stronger at WRESTRC than at RIM Park, which indicates that it is a more viable site. However, the terrain is also more complex at WRESTRC than at RIM Park. At WRESTRC, when the wind flowed from a non-dominant direction, it traveled over trees or buildings. During these times, the wind shear and turbulence intensity were significantly higher. When dealing with trees or buildings, a wind turbine should be placed above their boundary layer or far enough away to avoid detrimental flow conditions.

Chapter 6

Recommendations

The quality of data collected can be improved with better instrumentation. The current anemometers and vanes only measure the horizontal wind speed and wind direction. However, knowing the vertical component of wind velocity is important as well. A simple solution would be to install a propeller-type anemometer designed to capture the vertical axis, such as the R.M. Young 27106 sensor [48]. A more elegant option would be to install an ultrasonic anemometer that captures all three axes simultaneously, such as the R.M. Young 81000 sensor [48]. Both models are shown in Figure 6.1.

(a) RMY 27106 (b) RMY 81000

Figure 6.1: Two potential anemometers that capture the vertical component of wind velocity [48]

Icing is another concern; it certainly affected the met tower sensors and will affect any wind turbines in the Waterloo region. A heated anemometer is recommended and should

be mounted at the highest height on the tower. Both NRG Systems and R.M. Young offer heated versions of some of their anemometers [47, 48]. An alternative option would be to install an icing sensor, such as the Campbell Scientific 0871LH1 [67], shown in Figure 6.2. The main component is a rod, half of which is exposed to the elements. The rod is vibrated by an electromagnetic coil, and as ice accumulates on the rod, the frequency of oscillation decreases, which can be measured.

Figure 6.2: Campbell Scientific 0871LH1 icing sensor [67]

For a more detailed investigation into wind shear, measurements should be taken at more heights and at higher heights, if possible. Having measurements at more heights would reduce regression uncertainties and enable regressions with more degrees of freedom. This could involve mounting additional booms and sensors on the tower, or using sonic-based or laser-based instruments to scan the wind speeds over a range of heights.

For a more detailed investigation into turbulence intensity, the sampling rate should be increased. The NRG Symphonie data logger was easy to set up, since it was designed as part of a package along with the sensors. However, it has a fixed 2-second sampling rate and 10-minute averaging interval. A third-party data logger would require more effort to set up, but could offer greater customization. The data logger would need at least six counter inputs and five analog inputs to accomodate the current set of sensors.

The next step in the W3 Wind Energy Project is to install a small wind turbine in the Waterloo region. By measuring the actual energy output of the turbine, the success of the wind resource assessment and the accuracy of predicted values such as capacity factor and annual energy production can be examined.

References

[1] T. J. Price. Blyth, James (18391906). http://www.oxforddnb.com/view/article/100957, Accessed June 1, 2013.

[2] N. Jenkins T. Burton, D. Sharpe and E. Bossanyi. *Wind energy handbook*. John Wiley & Sons, 2001.

[3] Office of Energy Efficiency. Improving energy performance in Canada - report to Parliament under the Energy Efficiency Act for the fiscal year 2010–2011. Technical report, Natural Resources Canada, 2011.

[4] J. Hamilton. Wind power generation. http://crcresearch.org/node/304, Accessed June 1, 2013.

[5] Ontario Power Authority - Feed-in Tariff Program. http://fit.powerauthority.on.ca/, Accessed June 1, 2013.

[6] L. Landberg J. Hojstrup E. L. Petersen, N. G. Mortensen and H. P. Frank. Wind power meteorology part I: Climate and turbulence. *Wind Energy*, 1:2–22, 1998.

[7] A. N. Celik. Energy output estimation for small-scale wind power generators using Weibull-representative wind data. *Journal of Wind Engineering and Industrial Aerodynamics*, 91:693–707, 2003.

[8] J. V. Seguro and T. W. Lambert. Modern estimation of the parameters of the Weibull wind speed distribution for wind energy analysis. *Journal of Wind Engineering and Industrial Aerodynamics*, 85:75–84, 2000.

[9] T. P. Chang. Performance comparison of six numerical methods in estimating Weibull parameters for wind energy application. *Applied Energy*, 88:272–282, 2011.

[10] *IEC 61400-1 Wind turbines - Part 1: Design requirements*, 3rd edition, 2006.

[11] E. Prieto A. Garcia, J. L. Torres and A. De Francisco. Fitting wind speed distributions: a case study. *Solar Energy*, 62:139–144, 1998.

[12] A. N. Celik. Assessing the suitability of wind speed probability distribution functions based on wind power density. *Renewable Energy*, 28:1563–1574, 2003.

[13] M. Li and X. Li. MEP-type distribution function: a better alternative to Weibull function for wind speed distributions. *Renewable Energy*, 30:1221–1240, 2005.

[14] P. Ramirez and J. A. Carta. The use of wind probability distributions derived from the maximum entropy principle in the analysis of wind energy. *Energy Conversion and Management*, 47:2564–2577, 2006.

[15] O. A. Jaramillo and M. A. Borja. Wind speed analysis in La Ventosa, Mexico: a bimodal probability distribution case. *Renewable Energy*, 29:1613–1630, 2004.

[16] C. R. B. Filhoand L. A. Lima. Wind energy assessment and wind farm simulation in Triunfo - Pernambuco, Brazil. *Renewable Energy*, 35:2705–2713, 2010.

[17] A. H. Monahan and Y. He. The probability distribution of land surface wind speeds. *Journal of Climate*, 24:3892–3909, 2011.

[18] D. Weisser and T. J. Foxon. Implications of seasonal and diurnal variations of wind velocity for power output estimation of a turbine: a case study of Grenada. *International Journal of Energy Research*, 27:1165–1179, 2003.

[19] A. L. Rogers M. L. Ray and J. G. McGowan. Analysis of wind shear models and trends in different terrains. In *Proceedings of American Wind Energy Association Windpower 2006*, Pittsburgh, Pennsylvania, 2006.

[20] G. P. van den Berg. Wind turbine power and sound in relation to atmospheric stability. *Wind Energy*, 11:151–169, 2008.

[21] S. M. Pedersen M. S. Courtney R. Wagner, I. Antoniou and H. E. Jorgensen. The influence of the wind speed profile on wind turbine performance measurements. *Wind Energy*, 12:348–362, 2009.

[22] S. M. Pedersen I. Antoniou and P. B. Enevoldsen. Wind shear and uncertainties in power curve measurement and wind resources. *Wind Engineering*, 33:449–468, 2009.

[23] F. M. White. *Fluid Mechanics*. McGraw-Hill, 5th edition, 2002.

[24] S. Rehman and N. M. Al-Abbadi. Wind shear coefficient, turbulence intensity and wind power potential assessment for Dhulom, Saudi Arabia. *Renewable Energy*, 33:2653–2660, December 2008.

[25] J. G. Eisenhauer. Regression through the origin. *Teaching Statistics*, 25:76–80, 2003.

[26] S. T. Frandsen R. J. Barthelmie and M. N. Nielsen. Modelling and measurements of power losses and turbulence intensity in wind turbine wakes at Middelgrunden offshore wind farm. *Wind Energy*, 10:517–528, 2007.

[27] Siemens wind turbine SWT-2.3-82 VS. http://www.energy.siemens.com/mx/pool/hq/power-generation/wind-power/E50001-W310-A123-X-4A00_WS_SWT-2.3-82%20VS_US.pdf, Accessed June 1, 2013. product brochure.

[28] International Electrotechnical Commission. *IEC 61400-12-1 Power performance measurements of electricity producing wind turbines*, 2005.

[29] National Instruments. Wind turbine control methods. http://zone.ni.com/devzone/cda/tut/p/id/8189, Accessed June 1, 2013.

[30] M. J. Moran and H. N. Shapiro. *Fundamentals of engineering thermodynamics*. John Wiley & Sons, 5th edition, 2003.

[31] S. Kwon. Uncertainty analysis of wind energy potential. *Applied Energy*, 87:856–865, 2010.

[32] P. Ramirez and J. A. Carta. Influence of the data sampling interval in the estimation of the parameters of the Weibull wind speed probability density distribution: a case study. *Energy Conversion and Management*, 46:24192438, 2005.

[33] RETScreen International. *RETScreen Software Online User Manual*, 2012.

[34] N. Boccard. Capacity factor of wind power realized values vs. estimates. *Energy Policy*, 37:2679–2688, 2009.

[35] J. W. Rogers A. L. Rogers and J. F. Manwell. Uncertainties in results of measure-correlate-predict analyses. In *Proceedings of American Wind Energy Association Windpower 2005*, Denver, Colorado, 2005.

[36] S. Chatterjee and A. S. Hadi. *Regression analysis by example*. John Wiley & Sons, 4th edition, 2006.

[37] J. W. Rogers A. L. Rogers and J. F. Manwell. Comparison of the performance of four measure-correlate-predict algorithms. *Journal of Wind Engineering and Industrial Aerodynamics*, 93:243264, 2005.

[38] P. J. M. Clive. Non-linearity in MCP with Weibull distributed wind speeds. *Wind Engineering*, 32:319–324, 2008.

[39] R. Garcia-Rojo. Algorithm for the estimation of the long-term wind climate at a meteorological mast using a joint probabilistic approach. *Wind Engineering*, 28:213–224, 2004.

[40] UW Weather Station. http://weather.uwaterloo.ca/, Accessed June 1, 2013.

[41] National Climate Data and Information Archive. http://climate.weatheroffice.gc.ca/climateData/canada_e.html, Accessed June 1, 2013.

[42] D. Leick. Innovations in wind power technology. *Renewable Energy Focus*, 11(2):24–35, 2010.

[43] T. Kutney. Garrad Hassan: Wind farm design - an overview. Presentation, September 28, 2009. DC 1304, University of Waterloo.

[44] A. L. Rogers M. A. Lackner and J. F. Manwell. Uncertainty analysis in wind resource assessment and wind energy production estimation. In *Proceedings of the 45th AIAA Aerospace Sciences Meeting and Exhibit*, Reno, Nevada, 2007.

[45] K. Moyer. W3 wind energy feasibility study. Technical report, City of Waterloo, 2011.

[46] Regional Municipality of Waterloo Communities Orthoimagery. Via University of Waterloo map library, 2009.

[47] NRG Systems. http://www.nrgsystems.com/, Accessed June 1, 2013.

[48] R.M. Young Company. http://www.youngusa.com/, Accessed June 1, 2013.

[49] NRG Systems. *Symphonie data logger and accessories user's manual*, 2006.

[50] Campbell Scientific. *R.M. Young wind monitors instruction manual*, 2007.

[51] L. Landberg J. Hojstrup E. L. Petersen, N. G. Mortensen and H. P. Frank. Wind power meteorology part II: Siting and models. *Wind Energy*, 1:55–72, 1998.

[52] W. D. Lubitz. Effects of tower shadowing on anemometer data. In *Proceedings of the 11th Americas Conference on Wind Engineering*, San Juan, Puerto Rico, 2009.

[53] A. Bale S. Orlando and D. A. Johnson. Experimental study of the effect of tower shadow on anemometer readings. *Journal of Wind Engineering and Industrial Aerodynamics*, 99:1–6, 2011.

[54] P. R. Kenyon and D. C. Blittersdorf. Accurate wind measurements in icing environments. Technical report, NRG Systems, 1996.

[55] J. C. Wyngaard. Cup, propeller, vane, and sonic anemometers in turbulence research. *Ann. Rev. Fluid Mech.*, 13:399–423, 1981.

[56] O. Parent and A. Ilinca. Anti-icing and de-icing techniques for wind turbines: Critical review. *Cold Regions Science and Technology*, 65:88–96, 2011.

[57] T. F. Pedersen. On wind turbine power performance measurements at inclined airflow. *Wind Energy*, 7:163176, 2004.

[58] T. Ekelund. Yaw control for reduction of structural dynamic loads in wind turbines. *Journal of Wind Engineering and Industrial Aerodynamics*, 85:241–262, 2000.

[59] K. Briggs. Uncertainties related to the use of remote sensing data in wind resource assessments. In *Canadian Wind Energy Association Annual Conference and Exhibition 2009*, Toronto, Ontario, 2009.

[60] Southwest Windpower. http://windenergy.com/, Accessed June 1, 2013.

[61] Endurance Wind Power. http://www.endurancewindpower.com/, Accessed June 1, 2013.

[62] Sonkyo Energy. http://usa.windspot.es/, Accessed June 1, 2013.

[63] Bergey Windpower. http://www.bergey.com/, Accessed June 1, 2013.

[64] Wind Energy Solutions. http://www.windenergysolutions.nl/, Accessed June 1, 2013.

[65] Seaforth Energy. http://seaforthenergy.com/, Accessed June 1, 2013.

[66] Statistics Canada. *Households and the Environment: Energy Use*, 2007. Catalogue no. 11-526-S.

[67] Campbell Scientific 0871LH1. http://www.campbellsci.com/0871lh1-overview, Accessed June 1, 2013.

[68] J. G. McGowan J. F. Manwell and A. L. Rogers. *Wind energy explained*. John Wiley & Sons, 2nd edition, 2009.

[69] M. LeBlanc K. Harman E. Rareshide A. Tindal, C. Johnson and A. Graves. Site-specific adjustments to wind turbine power curves. In *American Wind Energy Association Windpower 2008*, Houston, Texas, 2008.

APPENDICES

Appendix A

Equipment data

Ch.	Sensor	Serial No.	Height	Scale	Offset
1	NRG #40C anemometer	179500069659	50m	0.758	0.39
2	NRG #40C anemometer	179500069464	40	0.760	0.31
3	NRG #40C anemometer	179500070249	40	0.758	0.37
4	NRG #40C anemometer	179500069592	30	0.758	0.35
5	NRG #40C anemometer	179500070307	20	0.757	0.35
6	RMY 05103 anemometer	88324	50	0.098	0
7	NRG #200P wind vane	–	30	0.351	0
8	RMY 05103 wind vane	88324	50	0.351	0
9	–	–	–	–	–
10	iPack/GSM voltmeter	38604590	1	0.021	0
11	NRG #110S temperature sensor	–	1	0.136	-86.383
12	NRG #BP20 pressure sensor	18056692	1	0.426	650.031
–	NRG Symphonie data logger	309018853	1	–	–

Table A.1: WRESTRC meteorological tower equipment data

Ch.	Sensor	Serial No.	Height	Scale	Offset
1	NRG #40C anemometer	179500070294	50m	0.757	0.36
2	NRG #40C anemometer	179500069485	40	0.758	0.36
3	NRG #40C anemometer	179500069655	40	0.756	0.40
4	NRG #40C anemometer	179500069589	30	0.759	0.36
5	NRG #40C anemometer	179500069651	20	0.759	0.34
6	RMY 05103 anemometer	88323	50	0.098	0
7	NRG #200P wind vane	–	30	0.351	0
8	RMY 05103 wind vane	88323	50	0.351	0
9	NRG #110S temperature sensor	–	1	0.136	-86.383
10	–	–	–	–	–
11	NRG #BP20 pressure sensor	18056691	1	0.426	647.694
12	iPack/GSM voltmeter	38604591	1	0.021	0
–	NRG Symphonie data logger	309018854	1	–	–

Table A.2: RIM Park meteorological tower equipment data

Instrument	Scale	Offset	Range
NRG #40C anemometer	0.765	0.35	1 to 96 m/s
RMY 05103 anemometer	0.098	0	1 to 60 m/s
NRG #200P wind vane	0.351	0	0 to 360 deg
RMY 05103 wind vane	0.351	0	0 to 360 deg
NRG #110S temperature sensor	0.136	-86.38	-40 to 52.5 °C
NRG #BP20 pressure sensor	0.4255	650	650 to 1086 mB

Table A.3: Default instrument calibration curves [49, 50]

Appendix B

MATLAB Code

```
function varargout = data_check(varargin)
% First variable is the reference
% Eliminate data that falls too far from reference
ref = varargin{1};
for n = 2:nargin;
    avg = varargin{n};
    d = nanmean(avg - ref);
    temp = zeros(length(avg),1);
    for i = 1:1:length(avg);
        upper = ref(i) + (d>0)*d/4 + (ref(i)+1)/4;
        lower = ref(i) + (d<0)*d/4 - (ref(i)+1)/4;
        if (avg(i) > upper) || (avg(i) < lower)
            temp(i) = NaN;
        else
            temp(i) = avg(i);
        end;
    end;
    varargout{n-1} = temp;
end;
end

function [k l] = weibfit(U)
% U = wind speed data
% k = shape factor
% l = scale factor
N = length(U);
k = 2;
```

```
k0 = 0;
while (abs(k-k0) > 0.001)
    k0 = k;
    t1 = U.^k0;
    t2 = log(U);
    k = 1/(nansum(t1.*t2)/nansum(t1) - nansum(t2)/N);
end;
l = (nansum(U.^k)/N)^(1/k);
end

function [a, z, b0, b1, b2, rmse1, rmse2, u_t1, u_t2] =
= eval_shear(h, u, h_t)
% h = row vector of heights
% u = matrix of wind speeds
% h_t = target height for wind shear extrapolation
% a = site roughness exponent
% z = site roughness length
% b0 = vector of roughness scale factors (2-param model)
% b1 = vector of roughness exponents (2-param model)
% b2 = vector of roughness exponents (1-param model)
% rmse1 = rms of regression errors (2-param model)
% rmse2 = rms of regression errors (1-param model)
% u_t1 = predicted wind speed at target height (2-param model)
% u_t2 = predicted wind speed at target height (1-param model)
% Site roughness parameters
u_mean = nanmean(u,1);
options = optimset('MaxFunEvals', 10000, 'MaxIter', 10000);
a = fminsearch(@powerlaw, 0.2, options, h, u_mean);
z = fminsearch(@loglaw, 2, options, h, u_mean);
% 10-minute roughness exponents
[n, j] = size(u);
b0 = NaN(n,1);
b1 = NaN(n,1);
b2 = NaN(n,1);
rmse1 = NaN(n,1);
rmse2 = NaN(n,1);
u_t1 = NaN(n,1);
u_t2 = NaN(n,1);
nans = 0;
for i = 1:n
    if (sum(isnan(u(i,:)))>0)
```

```
        nans=nans+1;
        continue;
    end;
    x = log(h/h(j));
    y = log(u(i,:)/u(i,j));
    [b0(i) b1(i) b2(i)] = lin_reg(x, y);
    e1 = u(i,:) - u(i,j) * (h/h(j)).^b1(i) * exp(b0(i));
    e2 = u(i,:) - u(i,j) * (h/h(j)).^b2(i);
    rmse1(i) = sqrt(sum(e1.^2)/j);
    rmse2(i) = sqrt(sum(e2.^2)/j);
    u_t1(i) = u(i,j) * (h_t/h(j)).^b1(i) * exp(b0(i));
    u_t2(i) = u(i,j) * (h_t/h(j)).^b2(i);
end;
end

function sse = powerlaw(a, h, u)
% a = roughness exponent (estimated)
% h = height
% u = wind speed
% sse = sum of squares of error (to be minimized)
h_ref = h(end);
u_ref = u(end);
u_fit = u_ref * (h / h_ref) .^ a;
err = u_fit - u;
sse = sum(err.^2);
end

function sse = loglaw(z0, h, u)
% z0 = roughness length (estimated)
% h = height
% u = wind speed
% sse = sum of squares of error (to be minimized)
h_ref = h(end);
u_ref = u(end);
u_fit = u_ref * log(h/z0) / log(h_ref/z0);
err = u_fit - u;
sse = sum(err.^2);
end

function [b0, b1, b2] = lin_reg(x, y)
% b0 = intercept (2-param)
```

```
% b1 = slope (2-param)
% b2 = slope (1-param)
xb = mean(x);
yb = mean(y);
n = length(x);
sxx = sum((x-xb).*(x-xb));
sxy = sum((x-xb).*(y-yb));
syy = sum((y-yb).*(y-yb));
b2 = sum(x.*y) / sum(x.*x);
b1 = sxy / sxx;
b0 = yb - b1*xb;
end

function turb = eval_turbulence(avgs, devs)
% avgs = Mean wind speed data
% devs = Standard deviation wind speed data
% turb = Long-term mean turbulence intensity
% Define constants
N_lim = 150; % number of data points in max time interval
i_lim = 1000;  % number of starting points
shift = 700;   % gap between start points
% Convert standard deviation to variance to make things easier
vars = devs.^2;
% Initialize
turb = zeros(N_lim,1);
for i = 1:i_lim;
    fprintf(1, '%5d\n', i);
    % Set the first entry
    run_avg = [avgs(1)];
    run_var = [vars(1)];
    turb_pt = sqrt(run_var(1))/run_avg(1);
    turb(1) = (1/i)*(turb(1)*(i-1) + turb_pt);
    for N = 2:N_lim;
        % Deal with NaNs
        if isnan(avgs(N))
            run_avg(N) = run_avg(N-1);
            run_var(N) = run_var(N-1);
        else
        % Formulas for average and variance
            run_avg(N) = (1/N) * ((N-1) * run_avg(N-1) + avgs(N));
            run_var(N) = (1/N) * ((N-1) * (run_var(N-1) +
```

```
            + (run_avg(N-1)-run_avg(N))^2) +
            + (vars(N) + (avgs(N)-run_avg(N))^2));
            turb_pt = sqrt(run_var(N))/run_avg(N);
            turb(N) = (1/i)*(turb(N)*(i-1) + turb_pt);
        end;
    end;
    % Move to a new starting point in time
    avgs = circshift(avgs, shift);
    vars = circshift(vars, shift);
    % Avoid landing on NaN
    while isnan(avgs(1))
        avgs = circshift(avgs, 1);
        vars = circshift(vars, 1);
    end;
end;
end

function [E0, Er, En] = eval_energy(U, P, T, rho, bins)
% U = wind speed data
% P = power curve
% T = time interval (aka, delta T)
% rho = density data
% bins = bin sizes to use
% E0 = AEP estimate using direct method
% Er = AEP estimate using direct method, density corrected
% En = AEP estimate using histogram method
% Direct method
% Use time series wind speed data
P0 = power_curve(U, P);
E0 = sum(P0)*T;
Pr = P0'.*rho;
Er = nansum(Pr)*T/1.225;
En = [];
% Histogram method
% Use histogram wind speed data
if ~isempty(bins);
    j = 0;
    for i = 1:length(bins);
        j = j+1;
        bin = bins(i);
        h = histc(U, 0:bin:ceil(max(U)/bin)*bin);
```

```
        Pn = power_curve((1:length(h))*bin-bin/2, P);
        En(j) = sum(h.*Pn')*T;
    end;
end;
end

function P = power_curve(U, pcurve)
% U = wind speed vector
% P = power vector
% pcurve = power curve matrix
pow_x = pcurve(:,1);
pow_y = pcurve(:,2);
for i = 1:length(U);
    if isnan(U(i)) || U(i)<min(pow_x) || U(i)>max(pow_x);
        P(i) = 0;
    else
        P(i) = interp1(pow_x, pow_y, U(i));
    end;
end;
end

function [m, b, sm, sb, R2, vm, vb] = mcp_method(x, y)
% m = slope (ordinary least squares)
% b = intercept (ordinary least squares)
% sm = error in slope (OLS)
% sb = error in intercept (OLS)
% R2 = correlation coefficient
% vm = slope (variance ratio)
% vb = intercept (variance ratio)
ns = isnan(x) + isnan(y);
x = x(~ns);
y = y(~ns);
xb = mean(x);
yb = mean(y);
n = length(x);
sxx = sum((x-xb).*(x-xb));
sxy = sum((x-xb).*(y-yb));
syy = sum((y-yb).*(y-yb));
m = sxy / sxx;
b = yb - m*xb;
sy = sqrt((syy-m^2*sxx)/(n-2));
```

```
sm = sy / sqrt(sxx);
sb = sy * sqrt(1/n + xb^2/sxx);
R2 = sxy^2/sxx/syy;
vm = sqrt(syy / sxx);
vb = yb - vm*xb;
end
```